



Analysis of the first 12 GHz PETS tests with beam using a constant parameter recirculation model

Erik Adli, University of Oslo and CERN*

Abstract

We analyse data from the first 12 GHz PETS tests with beam using a constant parameter recirculation model. The model is developed from basic principles and unknown parameters are estimated by fitting to measurements. The validity of the model is investigated by reconstructing RF power and phase from BPM data using the model and comparing the reconstructed signals with measured RF power and phase. Where applicable, disagreements between the reconstructions and the measurements are discussed, and possible explanations for the disagreements are suggested.

Geneva, Switzerland

April 14, 2009

*Work supported by the Research Council of Norway, the Swedish Research Council and the Wallenberg Foundation

This page is intentionally left blank.

Contents

1	Introduction	1
2	PETS power production	2
2.1	PETS longitudinal field without recirculation	2
2.2	PETS power production without recirculation	2
2.3	CTF3 beam characteristics and PETS fill	3
3	Recirculation model	4
3.1	Principle	4
3.2	Analytic expressions for pulses with constant intensity	4
3.3	Model parameters to be identified	5
3.4	Calculation of field for pulses with arbitrary intensity	6
3.5	Fast algorithm for pulses with arbitrary intensity	6
3.6	Example of reconstructed RF power and phase	7
4	TBTS measurements	9
4.1	BPM data	9
4.2	RF data	9
4.2.1	Diode measurement	9
4.2.2	I&Q channel measurement	10
5	Model fitting	12
5.1	Procedure	12
5.2	Timing adjustments	12
5.3	Fit metric	13
5.4	Fit result	13
6	Discussion of the fitted parameters	15
6.1	Splitter ratio	15
6.2	Constant factor and absolute power	16
7	Reconstruction of measured RF power	18
7.1	Pulses without pulse shortening	18
7.1.1	Example pulse	18
7.1.2	Pulses logged after klystron phase optimisation	19
7.1.3	Pulses logged before klystron phase optimisation	19
7.2	Pulses with pulse shortening	20
7.3	Phase fitting by varying recirculation phase for shortened pulses	21
8	Conclusions	29
8.1	Recommendations for future work	29
9	Acknowledgements	31

A	Estimation of the PETS output field and power	I
A.1	Basic concepts	I
A.2	Quantities defining a structure	I
A.3	PETS field amplitude	II
A.4	PETS output power	III
A.5	PETS integrated field	IV
A.6	Circuit-ohm convention versus linac-ohm convention	IV
A.7	Limitations and corrections to the simple expressions	V
	A.7.1 Structure length versus bunch-to-bunch spacing	V
	A.7.2 Single-bunch effects	V
A.8	Numerical estimations using PLACET	V
B	Example reconstruction using full GdfidL PETS model	VIII
C	Mapping between graph series number and data log folder names	IX
D	Reconstruction of additional pulses	X
D.1	More pulses logged after klystron phase optimisation	X
D.2	More pulses logged before klystron phase optimisation	XI
D.3	More pulses with pulse-shortening	XII
D.4	Pulses with three times combination after machine reset	XIII
E	Key plots without I&Q power	XV

1 Introduction

The first 12 GHz CLIC Power Extraction and Transfer Structure (PETS) [1] was tested with beam in the Two-Beam test stand (TBTS) [2] in the CLIC Test Facility 3 [3]. To be able to reach a relatively higher PETS RF power for the limited beam current, a field recirculator was conceived and fitted to the TBTS PETS [4]. The recirculator is equipped with a splitter, for adjusting the percentage of the field being recirculated, and a phase-shifter for adjusting the phase of the recirculated field. *Due to mechanical problems neither the splitter nor the phase-shifter could be remotely adjusted during the run, and the settings of neither were known a priori.* The average beam pulse intensity improved steadily during the 2008 TBTS PETS run (starting 14. November 2008), and all the measurements treated in this note are from the last day of operation, 11. December 2008. A sketch of the Two-Beam test stand with December 2008 configuration is depicted in Figure 1.

In this note we construct a model of the physics of the PETS equipped with a recirculator, using a *minimal* parameter set assuming constant recirculation phase, constant recirculation field split as well as constant PETS parameters. Except for the PETS fill-time, we do not consider other bandwidth limitations of the system in the model. This view-point resembles the "sausage model" approach used in e.g. the tracking code PLACET [5], and discussed further in Appendix A.

In order to test the model with the logged TBTS data it is necessary to first identify the unknown model parameters. We will then verify our model on a large number of measured pulses.

The advantage of such a minimal model, if proven successful, is that with simple tools one can get a good estimate of RF power and phase both in the transient and the steady state part of the RF pulse.

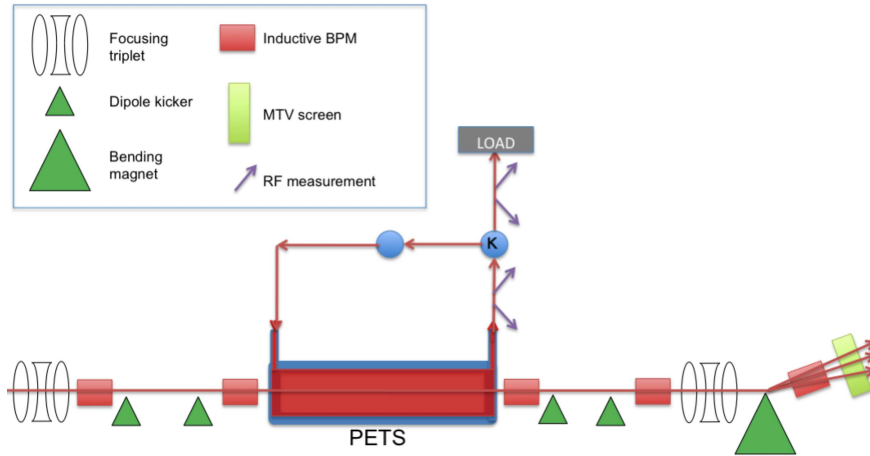


Figure 1: Sketch of the Two-Beam test stand (not to scale) - December 2008 configuration

2 PETS power production

2.1 PETS longitudinal field without recirculation

When the beam passes through the PETS it generates an electromagnetic field due to the impedance, oscillating with the fundamental mode frequency, f_{RF} , travelling with group velocity $\beta_g c$. The high group velocity implies some modifications to standard formulae [6] and Appendix A summarises useful PETS formulae. In steady state mode, if the structure is long with respect to the bunch spacing, the longitudinal field amplitude can be estimated as

$$E_{beam} = \frac{1}{2}(R'/Q)(2\pi f_{RF})\frac{L}{\beta_g c}IF(\lambda)\eta_{\Omega,PETS} \quad (1)$$

Table 1 describes the parameters of Eq. (1) and TBTS PETS values are given where applicable. Before the installation in the TBTS, the PETS was tested with a frequency analyser, showing almost perfect performance with a puny 9 MHz de-tuning, and 99.6% expected power production efficiency with respect to nominal performance [7].

Power parameters	Symbol	Value	Unit
PETS R'/Q per unit length	R'/Q	2222	Linac- Ω /m
PETS fundamental mode frequency	f_{RF}	12.0	GHz
PETS normalised group velocity	β_g	0.459	-
PETS active length	L	1.0	m
PETS ohmic losses reduction factor	$\eta_{\Omega,PETS}$	0.98	-
PETS de-tuning due to fabrication	Δf	9	MHz
PETS fill time	t_{fill}	4	ns
Average beam pulse intensity	I		A
Charge-distribution form factor	$F(\lambda)$		-
Beam generated field amplitude at PETS output	E_{beam}		V/m
RF power output from PETS	P		W

Table 1: Parameters relevant PETS for power production

Inserting beam parameters of e.g. $I=5$ A (about the maximum intensity in the PETS during this run) and $F(\lambda)=1$ (point-like bunch) we estimate the longitudinal field at the PETS output to $E_{beam} = 3.0$ MV/m.

2.2 PETS power production without recirculation

The longitudinal field and the power in the structure are related through R'/Q by $P = \frac{\beta_g c}{2\pi f_{RF}} \frac{E^2}{(R'/Q)}$ (see Appendix A). Steady state power production in a structure with high group velocity is thus given by

$$P = \frac{\pi}{2} (R'/Q) \frac{f_{RF}}{\beta_g c} I^2 L^2 F^2(\lambda) \eta_{\Omega, PETS}^2$$

which, for $I=5$ A and $F(\lambda)=1$, yields an estimated RF power of $P=7.3$ MW.

2.3 CTF3 beam characteristics and PETS fill

In the data analysed here (last day of TBTS run 2008) the CTF3 bunches are produced at 3 GHz, bypassing the delay loop, then combined with a factor two in the combiner ring before being extracted into the TL2, resulting in a CLEX beam ideally with $\bar{f}_{bunch}=6$ GHz. Figure 2 shows a pulse intensity measurement in the combiner ring. Figure 3 shows the actual bunch structure after recombination [8]. The logged pulses typically have lengths of about 300 ns.

The PETS output field is generated by the bunches in the time-slice of the beam given by the fill-time, defined here as the time between first RF at the output until steady state RF at the output is reached (see Appendix A). For beam-driven RF production with high group-velocity t_{fill} is calculated by¹

$$t_{fill} = \frac{L_{PETS}}{\beta_g c} (1 - \beta_g) = 4 \text{ ns} \quad (2)$$

and the corresponding number of bunches is $N_{fill} = t_{fill} \bar{f}_{bunch} \approx 24$ bunches. The finite PETS fill time can be seen as a low-pass filtering of RF power with respect to the pulse intensity, and this will be considered when we later reconstruct the RF power from a pulse intensity signal.

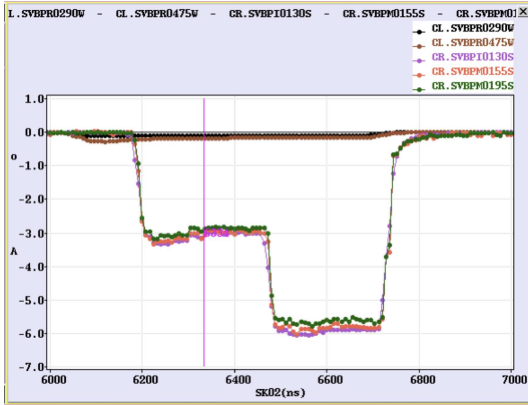


Figure 2: Example of a combined CTF3 pulse (from 11 December 2008)

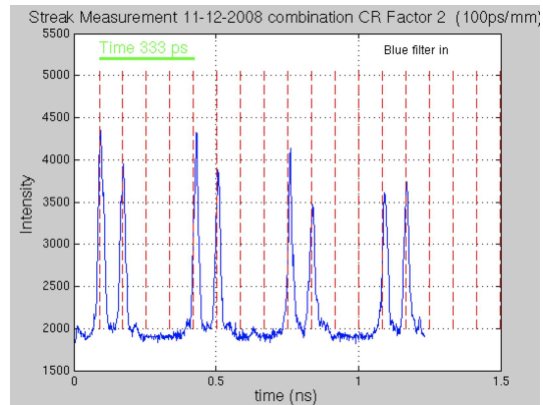


Figure 3: Example bunch structure in a combined beam (from 11 December 2008)

¹a factor $(1 - \beta_g)$ smaller than the fill-time of a RF-filled structure

3 Recirculation model

3.1 Principle

In the splitter a fraction of the PETS output field, κ , is coupled into the recirculation arm and will be coupled into the PETS at the input after a certain time. We define t_{circ} as the total round-trip time. $\eta_{\Omega,circ}$ denotes the field reduction factor due to ohmic losses after one round-trip (no precise estimate for this factor was available a priori). For notation simplicity we define the total gain factor of the field which is recirculated as $g = \kappa \eta_{\Omega,circ}$ (the splitter ratio and the ohmic losses act in the same way in this model). Depending on the effective length of the recirculation arm (adjustable by the phase-shifter) the recirculated field will in general be phase-shifted with respect to the beam generated field. We denote the phase-shift of the recirculation as ϕ . If at time m the field at the PETS output is E_m , this field will one recirculation cycle later add to the beam generated field, yielding a total field of

$$E_{m+1} = E_m g \exp(j\phi) + E_{beam}$$

If $\phi \neq 0$ the total field at the PETS output will in general not be in phase with the beam generated field, and we denote the total output field phase with respect to the beam generated phase by θ .

We summarise the recirculation parameters in Table 2.

Recirculation parameters	Symbol	Value	Unit
Splitter ratio (ratio of field entering recirculation arm)	κ		-
Ohmic losses reduction factor, round-trip	$\eta_{\Omega,circ}$		-
Total gain of circulated field after one round-trip	$g = \kappa \eta_{\Omega,circ}$		-
Recirculation round-trip time	t_{circ}		ns
Recirculation phase-shift (phase-error)	ϕ		rad
Total field at PETS output	E		V/m
Field phase with respect to the beam generated field	θ		rad

Table 2: Recirculator parameters

3.2 Analytic expressions for pulses with constant intensity

For steady state conditions with constant pulse intensity, I , we can find analytic expressions for the steady state amplitude and phase of the total field. The total field after M full recirculation cycles is

$$E_M = E_{beam} \sum_{m=0}^M g \exp(j\phi) \equiv E_{beam} \left\{ \frac{1 - g^{M+1} \exp(j(M+1)\phi)}{1 - g \exp(j\phi)} \right\} \quad (3)$$

The steady state solution $M \rightarrow \infty$ yields the field

$$\begin{aligned} E_{ss} &= \frac{E_{beam}}{1 - g \exp(j\phi)} = E_{beam} \left\{ \frac{1 - g \cos \phi}{1 - 2g \cos \phi + g^2} + j \frac{g \sin \phi}{1 - 2g \cos \phi + g^2} \right\} \\ &= \frac{E_{beam}}{\sqrt{1 - 2g \cos \phi + g^2}} \exp \left\{ \arctan \left(\frac{g \sin \phi}{1 - g \cos \phi} \right) \right\} \end{aligned} \quad (4)$$

and a steady state field phase

$$\theta_{ss} = \arctan \left\{ \frac{g \sin \phi}{1 - g \cos \phi} \right\}$$

For a perfect recirculation phase ($\phi = 0$) the steady state field reduces to

$$E_{ss} = \frac{E_{beam}}{1 - g}$$

$$\theta_{ss} = 0$$

After the beam has passed the PETS, assuming steady state has been reached, the field will decay according to

$$E_P = E_{ss} (g \exp(j\phi))^P \quad (5)$$

where P is the number of full recirculation cycles after the beam has passed.

Figures 4 and 5 show, in red, the power and phase corresponding to 5 A constant intensity beam pulses with point-like bunches, calculated using Eqs. (3) and (5) using a continuous running time. The recirculator settings used for the two figures are 1) $g=0.5$, $\phi=0$ (recirculating 50% of the field with no phase error) and 2) $g=0.75$, $\phi = 18^\circ$ (anticipating the identified recirculator settings for this run). The beam pulse intensity is indicated in green.

3.3 Model parameters to be identified

In our analysis we will assume that all the PETS and recirculator parameters in Table 1 and Table 2 stay constant. We do not take into account eventual bunch phasing errors (due to e.g. klystron pulse compression), nor varying bunch shape along the pulse. This implies that we can write the steady state field from the beam as $E_{beam} = cI$ where all the non-varying parameters have been lumped into the constant

$$c = \frac{1}{2} (R'/Q) (2\pi f_{RF}) \frac{L}{\beta_g c} F(\lambda) \eta_{\Omega, PETS} \quad (6)$$

When we later compare reconstructed power signals with measured, c will also take into account calibration errors in the measurements.

In this note we will assume the following values a priori unknown, and to be identified: the constant factor c , the recirculation gain g and the recirculation phase-shift ϕ .

3.4 Calculation of field for pulses with arbitrary intensity

The beam pulses during this CTF3 run vary in average intensity, and along each pulse the intensity might vary significantly as well. In order to compare the model and the CTF3 measurements this must be taken into account. We therefore write the generated field as $E_{beam}(t) = c\bar{I}(t)$ where $\bar{I}(t)$ is the average current of the $N_{fill} = t_{fill}f_{bunch}$ bunches responsible for the PETS output field at a given time t .

Introducing the notation $I_n \equiv I(t_n)$ for the beam pulse intensity sampled at time t_n , we can express the total field, including recirculation as

$$E_n = c \sum_{m=0}^M g^m \exp(jm\phi) \bar{I}_{n-am} \quad (7)$$

with $a = t_{circ}f_{BPM}$ and $M = a/N$, where f_{BPM} is the BPM sampling rate and N the number of the last valid intensity sample.

3.5 Fast algorithm for pulses with arbitrary intensity

Because the recirculator parameters are considered constant, the total field for a varying beam pulse can be computed relatively fast using a simple algorithm implementing Eq. (7). A Matlab/Octave example is given here :

```
% MAIN RECIRCULATION LOOP
% input: I_beam, delta_t, c, splitter_ratio, eta_ohm, phase, t_circ
t_pulse = length(I_beam)/delta_t;
E_mod_total = 0;
g = splitter_ratio*eta_ohm;
n_recirc_step = t_circ*delta_t;
M = ceil(t_pulse / t_circ);
for m=0:M,
    recirced_field = [zeros(1,round(n_recirc_step*m)) \
        c*(g*exp(j*phase))^m*I_beam(1,:)];
    E_mod_total = postpad(E_mod_total, length(recirced_field),0,2);
    E_mod_total += recirced_field;
end
E_mod_total = postpad(E_mod_total, length(I_beam_pad),0,2);
```

3.6 Example of reconstructed RF power and phase

For completeness we have included in Figures 4 and 5, in blue, the reconstructed RF pulses generated from rectangular pulses using the algorithm in the previous section for the two cases discussed in Section 3.2. The PETS fill-time, t_{fill} , has been taken into account, but the effect is barely visible for a rectangular pulse.

Finally, Figure 6 shows the steady state power and field phase as function of a varying recirculation phase ϕ with $g = 0.5$. By performing the same ϕ -scan with CTF3, TBTS measurements could be compared to these graphs in order to verify the recirculator operation. This would, however, require reasonably flat pulses.

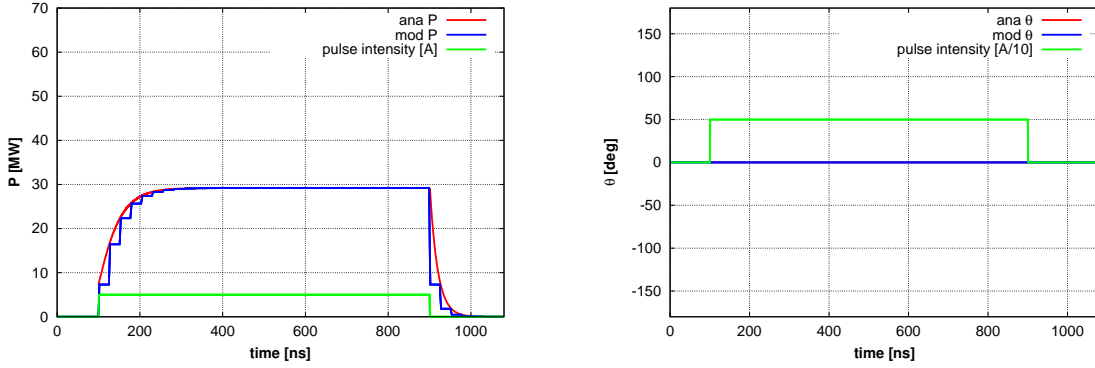


Figure 4: PETS output RF power (left) and PETS output field phase (right). Analytical expressions (in red) and reconstruction with algorithm from a rectangular beam pulse (in blue). The beam pulse is shown in green. Recirculator settings are $g=0.5$ and $\phi=0$ deg

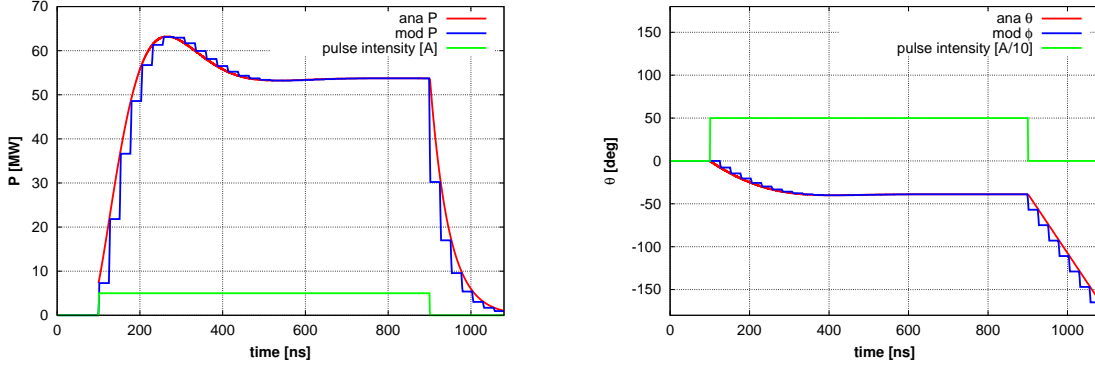


Figure 5: PETS output RF power (left) and PETS output field phase (right). Analytical expressions (in red) and reconstruction with algorithm from a rectangular pulse (in blue). The beam pulse is shown in green. Recirculator settings are $g=0.75$ and $\phi=-18$ deg

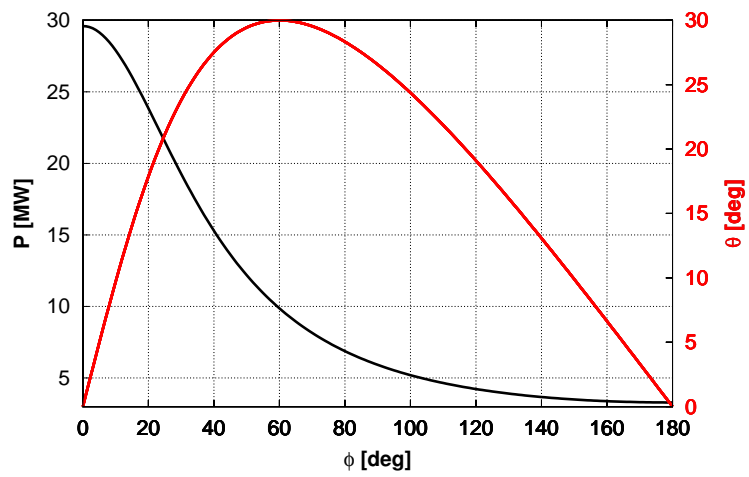


Figure 6: Steady state PETS output RF power (in black) and PETS field phase (in red) as function of varying recirculation phase

4 TBTS measurements

The TBTS is equipped with 5 inductive BPMs [9], as well as four RF measurement windows [10]. For each beam pulse, BPM data along the beam pulse and RF data along the RF pulse are stored. In this note we are primarily concerned with the BPM intensity (sum) signals for the BPM just in front of the PETS, and the RF window for the PETS forward power. The locations of these are indicated in Figure 7.

This section describes the instrumentation and the measurements, while in Section 7 RF pulses reconstructed from the BPM measurements, using the model presented in Section 3, will be compared to the measured RF pulses.

4.1 BPM data

The sum signal of the TBTS BPM has a bandwidth of 250 MHz [9]. The BPM read-out electronics has a sampling rate of 0.5 Gs/s, while the actual bandwidth is estimated to about 200 MHz, limited by the analog memory [11]. The BPM calibration was verified using a calibration current prior to the run.

We note that the time constant of the BPMs, $1/BW \approx 5$ ns, is about the same as the PETS fill-time of $t_{fill} \approx 4$ ns. In Eq. (7) we should therefore simply use $\bar{I}_k = I_k$ when reconstructing a power signal from the BPM reading (each BPM reading corresponds to a new fill of the PETS). In this analysis we will use data from the BPM just in front of the PETS, CM.BPM0370.

Figure 8 shows the CM.BPM0370 sum signal (corresponding to the pulse intensity) for an example pulse.

4.2 RF data

4.2.1 Diode measurement

The TBTS RF channels are equipped with diode RF power measurements, sampled by an Acqiris DC270 card with 8 bit digitisation, 1 Gs/s sampling rate and 250 MHz bandwidth [13]. The RF channels, including the diodes, were calibrated for the 2008 run, and the diode measurements therefore provide an absolute RF power reading. However, only linear calibration factors were available for the diode measurements and used in the analysis in this note.

Figure 10 shows the diode signal for the "PETS forward" channel, for the example pulse.

4.2.2 I&Q channel measurement

The TBTS RF channels are also equipped with I and Q demodulators (measuring the field with 90° relative phase), also sampled by Acquiris DC270 [13]. However, the I&Q signals were relatively weak and therefore spanned only a limited range of the 8 available digitisation bits, resulting in significant noise in form of spikes on these measurements. The signals were filtered through a optimal Savitzky-Golay filter (2nd order, 5 samples half-width) [14] which smoothes out sample to sample noise while preserving lower frequency part of the signal. The I and Q channels were not calibrated for the 2008 run, and thus provided only a relative power reading. The I&Q data were only available for the "PETS forward" channel for this run. However, the I&Q channels have the advantage that they provide measurements of the relative field phase.

Figure 9 shows both the raw and filtered I and Q channels, for the example pulse. From the I and Q channel the power is reconstructed as

$$P_{meas} = c_{IQ}(I^2 + Q^2)$$

and the field relative phase as

$$\theta_{meas} = \arctan(I/Q)$$

c_{IQ} was adjusted in order to fit the I&Q power to the calibrated diode power measurements at a level of around 17 MW ($c_{IQ} = 3.9 \times 10^4$). Figure 10 compares the two power measurements. Figure 11 shows the IQ phase measurement for the example pulse. The plots also contain the BPM beam intensity measurement for convenience.

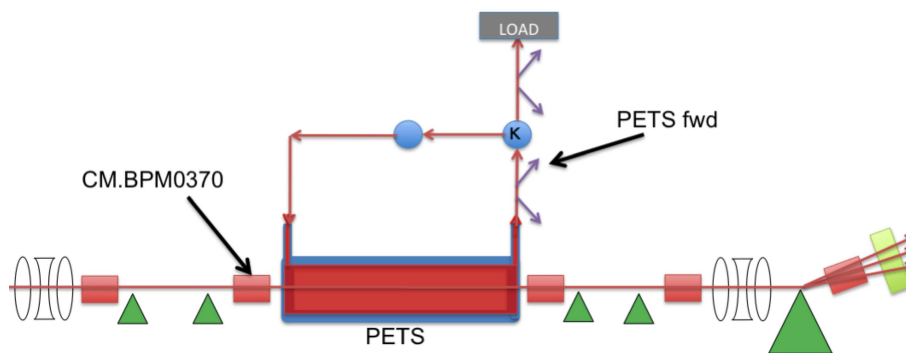


Figure 7: Locations of measurements used for the TBTS analysis

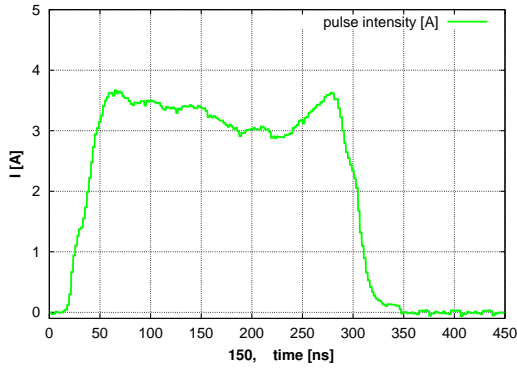


Figure 8: BPM intensity measurements for the example pulse

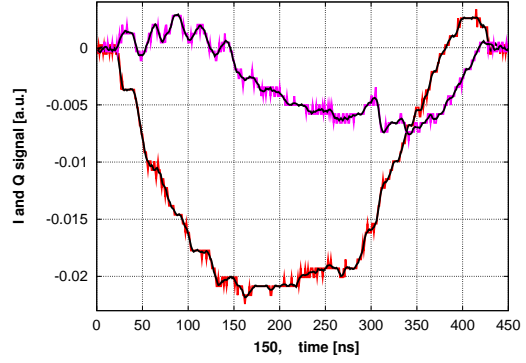


Figure 9: The I&Q channels showed separately for the example pulse. The I-channel in red, and the Q-channel in magenta. The filtered signals are also shown, in black

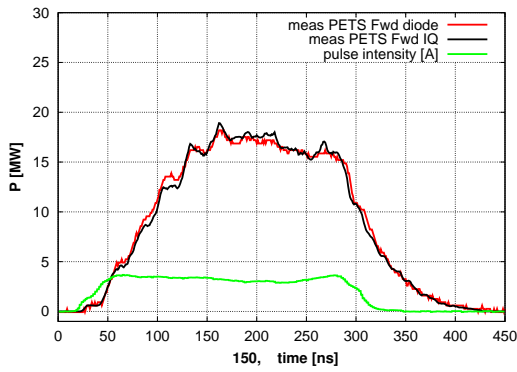


Figure 10: Diode power measurement (in red) and scaled I&Q channel power measurements (in black) for the example pulse. BPM intensity in green.

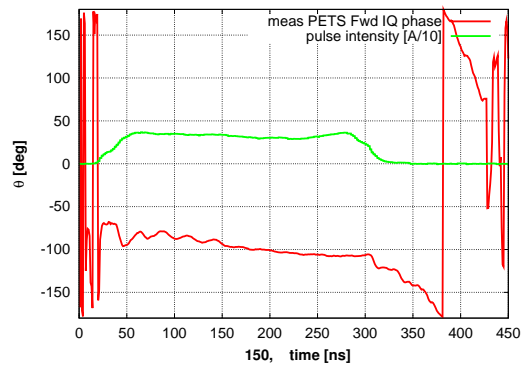


Figure 11: I&Q phase measurement for the example pulse, in red. BPM intensity in green.

5 Model fitting

5.1 Procedure

We will now verify the applicability of the minimal-parameter recirculation model described by Eq. (7), by using this equation to reconstruct RF power and phase using BPM intensity data as input. The reconstructed RF power and phase will then be compared with the ones measured from the I&Q channels.

Such a comparison is made more difficult by the fact that neither the recirculator gain g nor the phase-error ϕ were known during the run (and was neither possible to measure). In addition precise bunch length measurements were not available, and thus the charge form factor and consequently the constant c , were unknown. In order to compare the reconstructed RF to the measured we must therefore first fit three unknown parameters of the model, g , ϕ and c . A value $t_{circ} = 26$ ns was used in the fitting. This value was deduced by measuring the time between the power level steps in the measured RF data, as observed in e.g. Figure 10.

We seek to fit the three unknown parameters by defining a metric to compare the reconstructed and measured RF, and then scan the 3D parameters space for a global minimum. We use 200 subsequent pulses, of varying shape and amplitude as data to be fitted. The RF power amplitude varies from about 10 MW to 25 MW (according to the calibrated diode RF power measurement). The pulse series was logged in a period where no significant pulse-shortening was observed. Low power pulses corresponding to machine/klystron problems were automatically excluded from the fit. The I&Q channel signals were used for the reconstruction of both the power and the phase signal (alternatively the diode signal could have been used for the power fit, but it was seen as more consistent to use the I&Q channels for both).

5.2 Timing adjustments

The BPM measurements were not automatically synchronised in time to the RF measurements. As part of the fit algorithm the I&Q channel signals were therefore shifted in order to start at the same time as the BPM. The shift needed (time-scale of a few 10's of ns) was the same for most pulses (+/- one sample), but for a few pulses timing jitter was observed, and a different shift was needed.

In addition to the coarse timing fit, the measured RF phase was shifted to match the reconstructed phase at a temporal interval close to the start of the pulse. This adjustment, which we denote ψ , varied from pulse to pulse. The adjustment needed varied from about $\psi \approx 35^\circ$ to $\psi \approx 75^\circ$ (a time-scale of some 10's of ps). For reference Figure 12 shows the phase adjustment applied to each pulse (pulses excluded in fit are not shown). [15] includes a discussion of a different fitting procedure where ψ was allowed to vary along the pulses.

5.3 Fit metric

The following χ^2 metric was constructed

$$\chi^2(c, g, \phi) = \frac{1}{N_p} \Sigma \left\{ [P_{meas} - P_{mod}(c, g, \phi)]^2 / \hat{P}_{meas} + c_{P\theta} [\theta_{meas} - \theta_{mod}(c, g, \phi)]^2 \right\} / L_p$$

where N_p is the number of pulses, L_p the pulse-length and $c_{P\theta}$ a normalisation factor that gives the phase fit a weigh equal to the power fit.

5.4 Fit result

After scanning the parameter space, the following set was found to give a global minimum for χ^2

$$c = 0.78$$

$$g = 0.75$$

$$\phi = -18^\circ$$

where c is the scaling of the power reconstructed from the BPM intensity, assuming the nominal PETS parameters in Table 1 and a form factor of $F(\lambda) = 1$.

Figure 13 shows a fit surface for g and ϕ showing a global minimum. Figure 14 shows valleys in the parameters space for each of the three fitted parameters. The localisation of a clear region of minimum values indicates that the metric has been successful in locating a valid parameter fit. The figures also show the granularity of the parameter scan. We note that it was necessary to include the phase-fit in the metric in order to clearly locate a minimum; fitting the power alone did not yield a clear minimum.

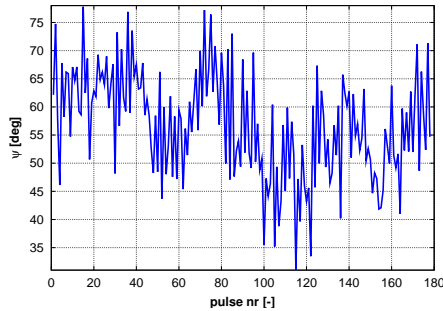


Figure 12: Pulse-by-pulse I&Q channel phase-shift, ψ , needed to fit the field phase θ

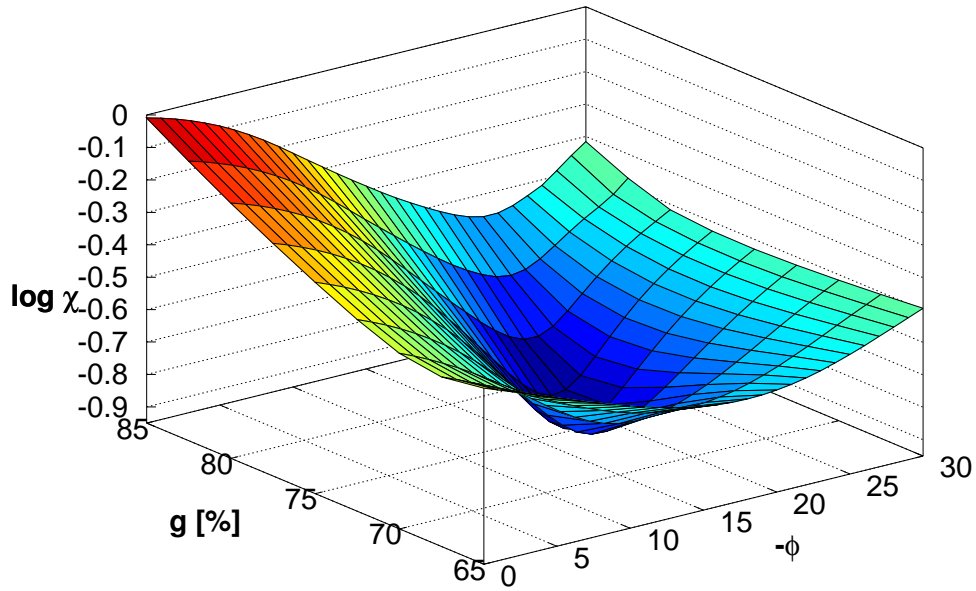


Figure 13: χ^2 fit results: one g, ϕ surface

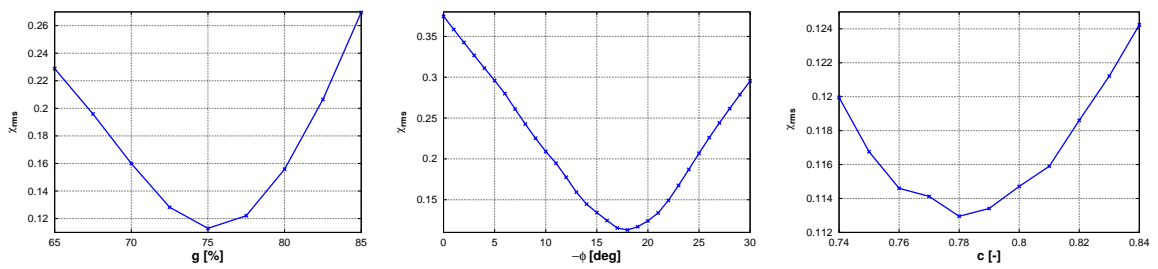


Figure 14: χ^2 fit results: g, ϕ, c valleys in the parameter space

6 Discussion of the fitted parameters

6.1 Splitter ratio

We have estimated the part of the field being recirculated to $g = 0.75$. The TBTS provides four RF windows, the PETS forward and reflected signals, as well as the ACC forward and reflected signals ("ACC" denoting "to an accelerating structure". However, for this run no accelerating structure was installed). Figure 15 shows the location of these windows. Figure 16 shows the corresponding diode measurements for a given pulse. From these data we will do a rough estimate of the splitter ratio, κ , and from that, together with our fitted value for g , estimate the ohmic losses reduction factor for one full circulation, $\eta_{\Omega,circ}$.

The picture is made more complicated by the small reflected signal (the "PETS refl" channel). In order to proceed we assume that the reflected signal originates from the mechanically stuck phase-shifter (this is plausible according to [12]). The parameter g we have identified can then be expressed as $g = \kappa \kappa_\phi \eta_{\Omega,circ}$ where we have defined κ_ϕ as the field transmission ratio through the phase-shifter. κ is the field transmission ratio from E_0 to E_1 , and also on the return path, from E_3 to E_6 . Furthermore, the field transmission to the fourth coupler port is given by $E_5^2 = (1 - \kappa^2)E_3^2$ [12].

With the notation defined in Figure 15, and considering energy flow preservation at the nodes, the splitter ratio can be estimated from e.g. Figure 16 as

$$\kappa^2 \equiv \frac{E_1^2}{E_0^2} = \frac{E_2^2 - E_0^2}{E_0^2} = 1 - \frac{ACC_{fwd}}{PETS_{fwd}} \approx 0.82$$

We then use the relation $(1 - \kappa_\phi^2)E_1^2 \equiv E_3^2$ to estimate

$$\kappa_\phi^2 = 1 - \frac{1}{\kappa^4} \frac{E_6^2}{E_0^2} = 1 - \frac{1}{\kappa^4} \frac{PETS_{refl}}{PETS_{fwd}} \approx 0.82$$

Other pulses yield similar results, and we can then do a rough estimate of the ohmic losses reduction factor, taking into account the reflection, as

$$\eta_{\Omega,circ} = \frac{g}{\kappa \kappa_\phi} \approx 0.91$$

No a priori estimate was available for this value. In comparison, the ohmic losses reduction factor for the PETS alone is estimated to $\eta_{\Omega,PETS} = 0.98$ [12].

6.2 Constant factor and absolute power

We have estimated a scaling $c = 0.78$ needed to fit the power reconstructed from the BPM data, assuming a PETS with nominal parameters with a perfect beam with $F(\lambda) = 1$, to the power measured by the diode signal:

$$P_{mod|F(\lambda)=1} = c^2 P_{meas} = (0.78)^2 P_{meas}$$

From Eq. (6) we see that c contains the charge-distribution form factor, PETS design parameters, beam de-tuning, and will also be affected by erroneous calibration values. The form factor $F(\lambda)$, defined in Appendix A, depends on the RMS bunch-length, the shape of charge distribution and the RF frequency, and is for a Gaussian bunch given by $F(\lambda(\sigma_z)) = \exp(-2(\pi\sigma_z f_{RF}/c)^2)$.

If we assume perfect calibration factors, perfectly synchronous beam and perfect PETS then $c \equiv F(\lambda) = 0.78$, corresponding to a Gaussian RMS bunch length of 2.8 mm:

$$P_{mod|F(\lambda)=0.78} = P_{meas}$$

No drive beam bunch length measurements have been performed in the CLEX area so far, and no precise upstream bunch-length measurements were performed during the run analysed here either. Some measurements had been done before the run, indicating a relatively long bunch in CTF3 before the combiner ring (1.5 mm \approx 2 mm) [8]. Although rough, these numbers indicate that not all of the constant factor should be contributed to the bunch-length.

Can we still say something about how close the reconstructed power level is with respect to the RF measurements? If we assume that the bunch RMS length is as little as 1.5 mm, we need to scale the reconstructed power by a factor $c/F(1.5 \text{ mm}) = 0.84$ to match the measurements. If the bunch is actually longer the agreement between reconstruction and measurement will be better. We have also assumed when estimating c that the bunch frequency matches the PETS synchronous frequency perfectly. If the actual bunch phasing is not perfect the agreement will improve as well. This indicates, if we assume the BPM and RF diode calibration to be correct, that the agreement reconstructed and measured RF is at least $(1 - 0.84^2) \times 100\% \approx 30\%$.

This discussion shows, however, the importance of a precise RMS bunch-length measurements² in order to be able to precisely benchmark drive beam PETS operation.

²ideally it is the form factor itself that needs to be known, not only the RMS bunch-length

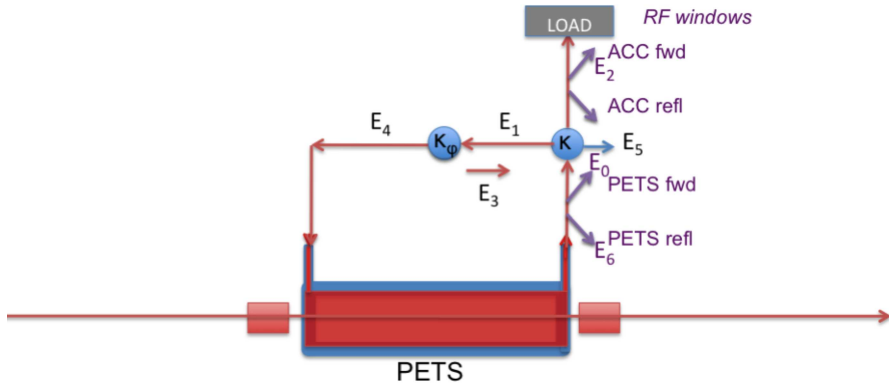


Figure 15: TBTS RF windows

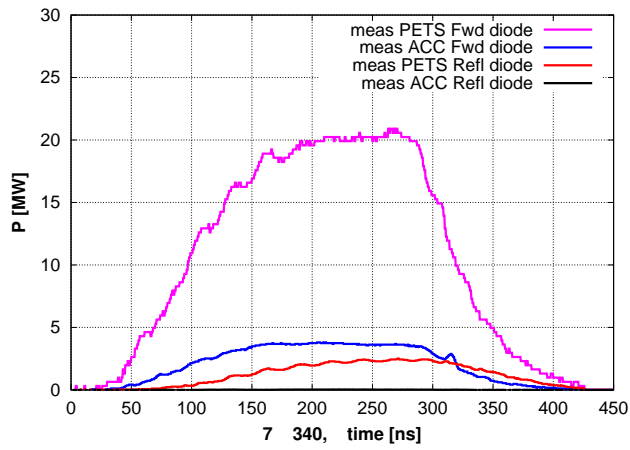


Figure 16: Diode power measurements for each RF window, for a typical pulse

7 Reconstruction of measured RF power

In this section we give examples of how the reconstructed RF power and phase compare to the measured, using the values for the unknown model parameters as estimated in Section 5. As an example we first discuss the measured pulse already showed in Section 4, Figures 10 to 11, which was also part of the pulses used for the parameter fit. Then we show how our model apply to various pulses not part of the fit, measured at different time of the day. Pulse series were logged semi-manually at certain points during the day. In order not to discriminate among the pulses shown we present the first two pulses in each series.

The power plots in the section contain both the diode and the I&Q power measurements since the purpose of this note is also to do a first benchmarking of the TBTS instrumentation. However, in Appendix E we have re-plotted several of the graphs with the diode power measurement only, for possible re-use of the graphs.

For book-keeping reasons all pulses are on the x-axis tagged with the log series number followed by the pulse number within that series. A mapping between the series number, the time of logging and the folder names for the logged data is given in Appendix C.

7.1 Pulses without pulse shortening

7.1.1 Example pulse

The pulse shown in Figure 17, part of the fit, was logged at 16:05.

The left graph shows the measured BPM pulse intensity in *green*, RF power reconstructed from the pulse intensity using the model in *blue*, the RF power diode measurement in *magenta* and the RF power I&Q measurement in *red*. The right graph shows the measured BPM pulse intensity in *green*, RF phase reconstructed from the pulse intensity using the model in *blue* and the RF power I&Q measurement in *red*. In the legend measurements are prefixed with "meas" and the reconstruction using the algorithm described in Section 3.5 is prefixed by "mod".

We observe that both the rise time and the fall time of the reconstructed power correspond to the measured power. The small scaling difference we believe is mainly due to a non-linearity of the power measurements as will be discussed in Section 7.1.2.

The reconstructed phase follows the measured, except at the start where the measured phase shows a more erratic behaviour. Our simple approach with a "sausage model" instant fill and drain-out of the field neglects some transient effects. Appendix B shows an example of a pulse reconstruction with recirculation using a single bunch response calculated using a complete GdfidL model. The phase shows an oscillatory behaviour, with a period equal to the recirculation time, until steady state is reached.

In general the reconstructed RF signal is much smoother than the measured. Part of this might be due to the sausage model used for reconstruction. However, the reconstructed signal is much smoother along all of the RF pulse, and not only at the first part of the pulse where phase oscillations are expected to be present (see Appendix B). This might indicate that the actual bandwidth of the BPMs is lower than the reported 200 MHz.

We conclude that for this pulse the fit gives a model reconstruction which is to a high degree consistent with the measured RF, and where plausible explanations for the major disagreements exist.

7.1.2 Pulses logged after klystron phase optimisation

The CTF3 machine was constantly being tuned between the logging of RF data, and during the day significant changes in machine working point took place. The pulses discussed in this subsection are all from a period of about three hours (14:20 to 16:15) when the CTF3 machine was running more or less in the same condition. Note that none of the pulses presented in this note, except the one in the last paragraph, were part of the set of pulses used for the fit.

The first two pulses of the 16:02 series are shown in Figures 18 and 19.

The first two pulses of the 15:48 series are shown in Figures 20 and 21.

Some high-power pulses with different intensity shape from the 16:02 series are shown in Figures 22 and 23. We observe how the I&Q derived power level is often significantly different from both the diode and the reconstruction, higher for high power level and lower for low power level. The phase fits reasonably well. This might indicate a relatively strong non-linearity in the I&Q channel measurements. Observing the diode signal, however, we observe that the RF reconstruction correctly takes into account the different beam intensity shape of the two pulses.

The pulse with the highest power level logged is shown in Figure 24. Both the reconstructed and the diode measurements indicate a power level of about 30 MW. The much sharper fall-off of the measured power and phase with respect to the reconstruction could be explained by pulse-shortening (see Section 7.2).

More reconstructed pulses logged in the same period (14:20 to 16:15) are shown in Appendix D.1. They all show reasonable agreement between reconstruction and measurement.

7.1.3 Pulses logged before klystron phase optimisation

The first two pulses of the 13:23 series are shown in Figures 25 and 26.

We see that for these pulses (and the subsequent in the series) the parameters fit based on data from the 16:02 series does not give a good correspondence anymore. The roll-off of the power level is much more significant, and the field phase does not fit well either. Applying a new fit for these pulses gives a new minimum of $g = 0.825$ and $\phi = 30^\circ$, however these parameters do not give a good agreement between reconstruction and measurement either. There are *no* parameters that allow such fast roll-off while preserving anything close to the measured field phase. The physics of these pulses are thus not well described by our simple model.

More reconstructed pulses, from the start of the logging up to about one hour earlier than the 13:23 series, are shown in Appendix D.2. They show clearly the same characteristics as the 13:23 series.

One possible explanation for this discrepancy could be significant distortions in the the bunch phasing for the logged pulse in these series, leading to modulation of the produced power. This theory is supported to some extent by the fact that the CTF3 klystron phases were reported optimised [16] between the series at 13:23 (the last series were the reconstruction does not compare well) and the later runs (were the reconstruction compares well).

Also supporting this theory is the fact that many of the pulses logged before the reported klystron phase optimisation show a continuous oscillation of the field phase. A possible explanation for this is that the RF field steady state regime is not reached in the PETS due to non-ideal bunch phasing, in contrast to the ideal simulated case in Appendix B.

To quantify the effect of the klystron phases in order to draw final conclusions, further investigations would be needed, including thorough studies of the effect of klystron phases on the bunch phasing (possibly involving detailed simulations of the CTF3 beam dynamics).

7.2 Pulses with pulse shortening

During part of the run there were time spans where a large fraction of the RF pulses were much shorter than they should according to the BPM intensity (or the reconstructed pulses). This pulse-shortening is believed to be due to break down in the PETS or the wave guides. It is not the purpose of this note to go into details about the eventual break downs, but we will show here how the pulse-shortening also affects the measured I&Q phase. Figures 27, 28 and 29 show some typical pulses where a pulse-shortening is observed (these pulses were logged after the reported optimisation of the klystron phases was performed).

More reconstructed pulses with pulse-shortening are shown in Appendix D.3. We conclude that for pulses with pulse-shortening both the RF power and phase deviate significantly from the model values. The field phase varies in a number of different ways;

sharp decline, sharp rise or oscillations.

7.3 Phase fitting by varying recirculation phase for shortened pulses

For shortened pulses it is of interest to understand the origin of the pulse-shortening, as a way to aide the understanding of RF break downs. One approach that was suggested [12] was to verify whether the pulse-shortening could be explained by varying the recirculation phase alone. The idea is that break down products such as plasma can introduce parasitic RF phase delay.

For the first pulse in the last paragraph we will fit the measured field phase, θ , by introducing a "dip" in the recirculation phase, ϕ , as shown in Figure 30. The resulting RF power and phase are shown in Figure 31. The reconstructed field phase is now following the measured phase closely. The reconstructed power is lower due to the phase-dip, but still significantly higher than the measured. This indicates that for this pulse a recirculation phase-change alone cannot reconstruct the RF signal.

If we in addition introduce a change in recirculator gain, g , along the pulse it is clear that the power can be fitted as well. More elaborate theories of break down could support the physical meaning of such fits, but since this note does not aspire to investigate the physics of break down we end the discussion here with the phase fitting null result.

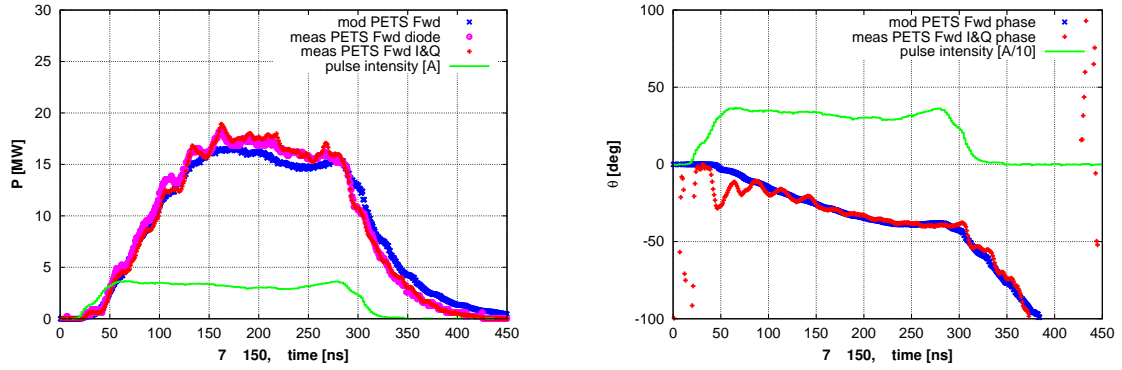


Figure 17: The example pulse. Reconstructed and measured RF power (left) and phase (right). Reconstruction using the model in blue (x). Diode power signal in magneta (o). I&Q channel signals in red (+). BPM intensity in green (-).

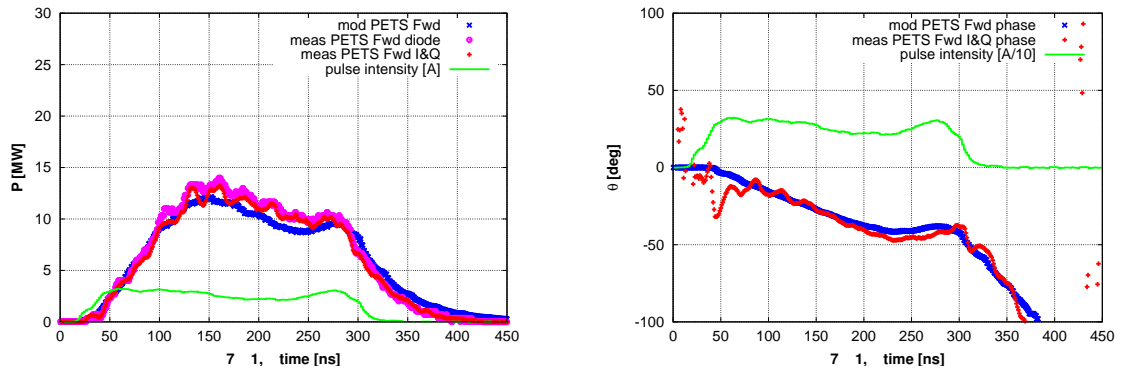


Figure 18: First pulse from the 16:02 series. Reconstructed and measured RF power (left) and phase (right). Reconstruction using the model in blue (x). Diode power signal in magneta (o). I&Q channel signals in red (+). BPM intensity in green (-).

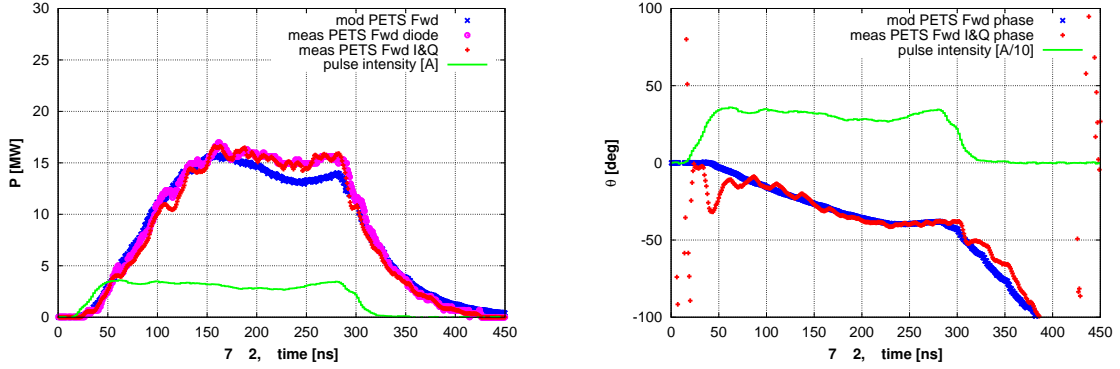


Figure 19: Second pulse from the 16:02 series. Reconstructed and measured RF power (left) and phase (right). Reconstruction using the model in blue (x). Diode power signal in magneta (o). I&Q channel signals in red (+). BPM intensity in green (-).

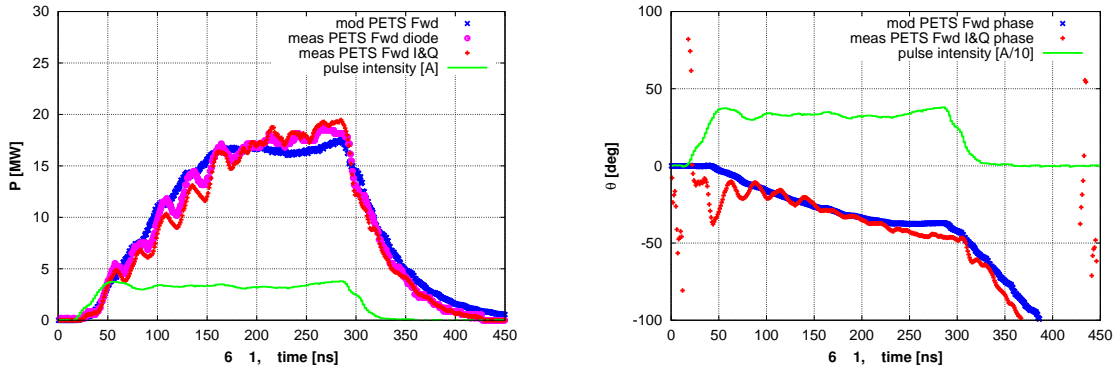


Figure 20: First pulse from the 15:48 series. Reconstructed and measured RF power (left) and phase (right). Reconstruction using the model in blue (x). Diode power signal in magneta (o). I&Q channel signals in red (+). BPM intensity in green (-).

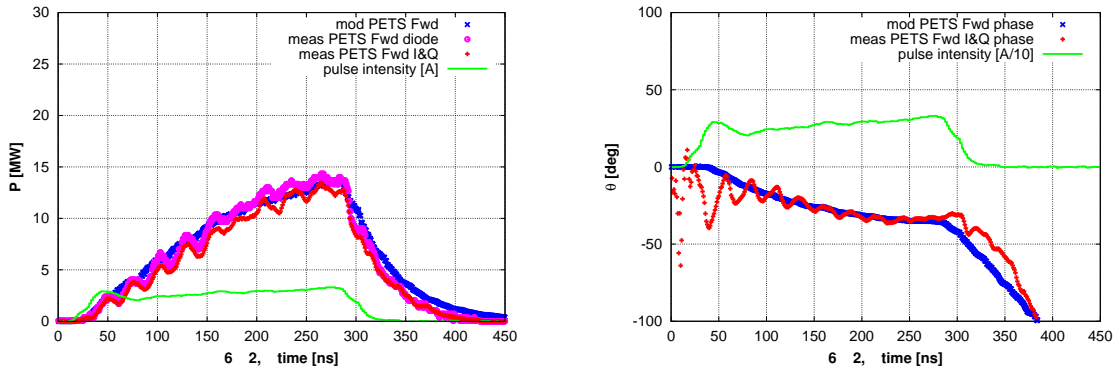


Figure 21: Second pulse from the 15:48 series. Reconstructed and measured RF power (left) and phase (right). Reconstruction using the model in blue (x). Diode power signal in magneta (o). I&Q channel signals in red (+). BPM intensity in green (-).

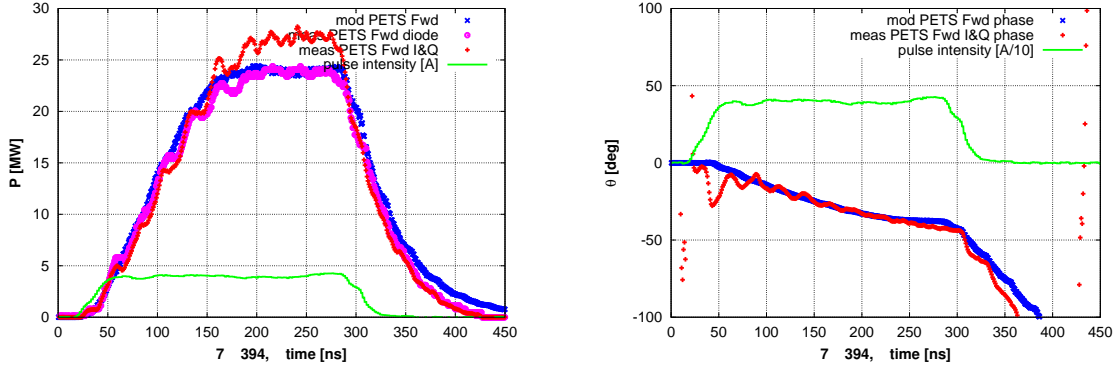


Figure 22: A high power, flat-top pulse from the 16:02 series. Reconstructed and measured RF power (left) and phase (right). Reconstruction using the model in blue (x). Diode power signal in magneta (o). I&Q channel signals in red (+). BPM intensity in green (-).

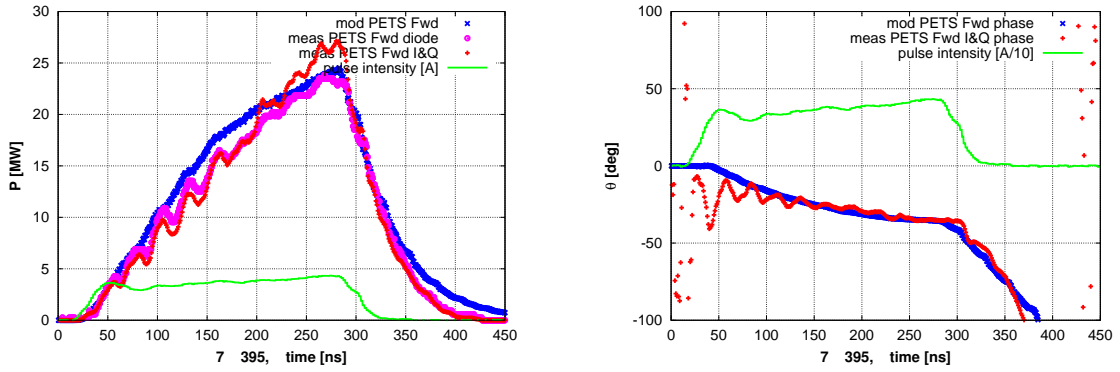


Figure 23: A high power, peaked pulse from the 16:02 series. Reconstructed and measured RF power (left) and phase (right). Reconstruction using the model in blue (x). Diode power signal in magneta (o). I&Q channel signals in red (+). BPM intensity in green (-).

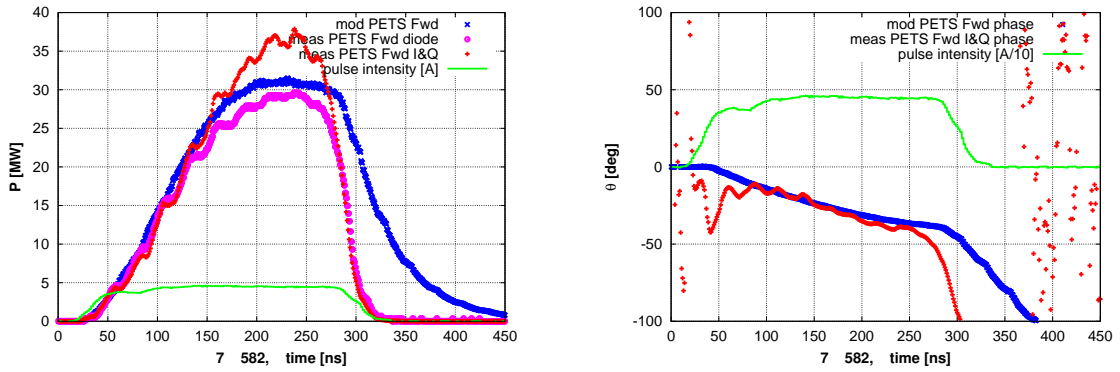


Figure 24: The pulse with the highest power logged. From the 16:02 series. Reconstructed and measured RF power (left) and phase (right). Reconstruction using the model in blue (x). Diode power signal in magneta (o). I&Q channel signals in red (+). BPM intensity in green (-).

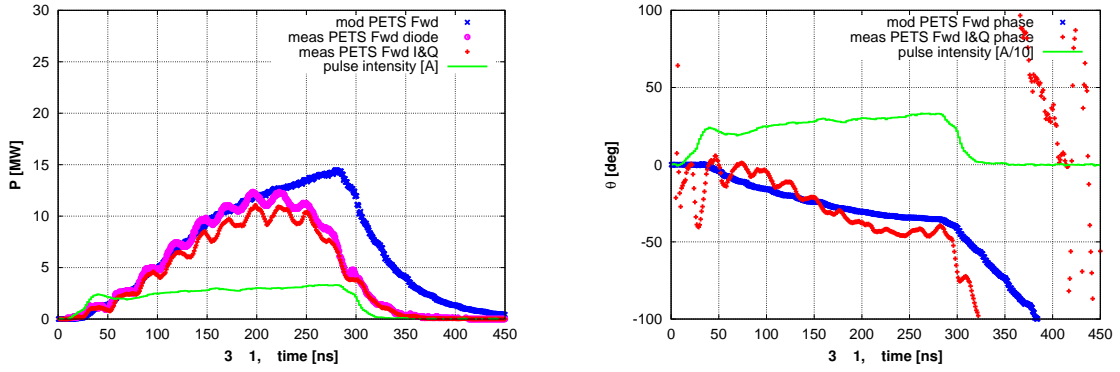


Figure 25: First pulse from the 13:23 series. In this series the correspondence reconstruction and measurement is not very good, possibly due to bunch phasing errors. Reconstructed and measured RF power (left) and phase (right). Reconstruction using the model in blue (x). Diode power signal in magneta (o). I&Q channel signals in red (+). BPM intensity in green (-).

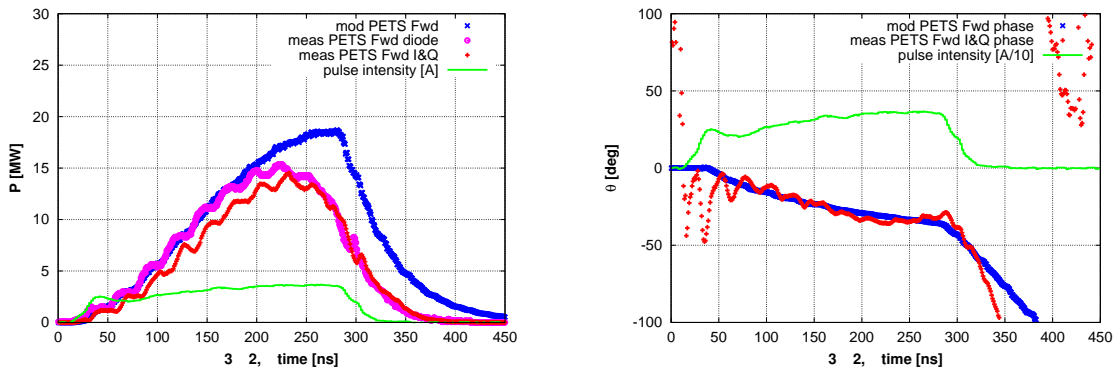


Figure 26: Second pulse from the 13:23 series. In this series the correspondence reconstruction and measurement is not very good, possibly due to bunch phasing errors. Reconstructed and measured RF power (left) and phase (right). Reconstruction using the model in blue (x). Diode power signal in magneta (o). I&Q channel signals in red (+). BPM intensity in green (-).

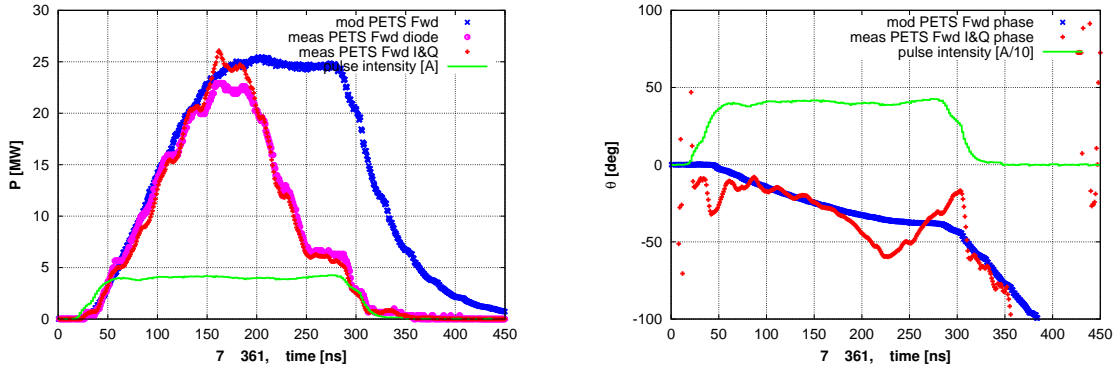


Figure 27: Pulse with pulse-shortening, with field phase sharply increasing around time of pulse-shortening. From the 16:02 series. Reconstructed and measured RF power (left) and phase (right). Reconstruction using the model in blue (x). Diode power signal in magneta (o). I&Q channel signals in red (+). BPM intensity in green (-).

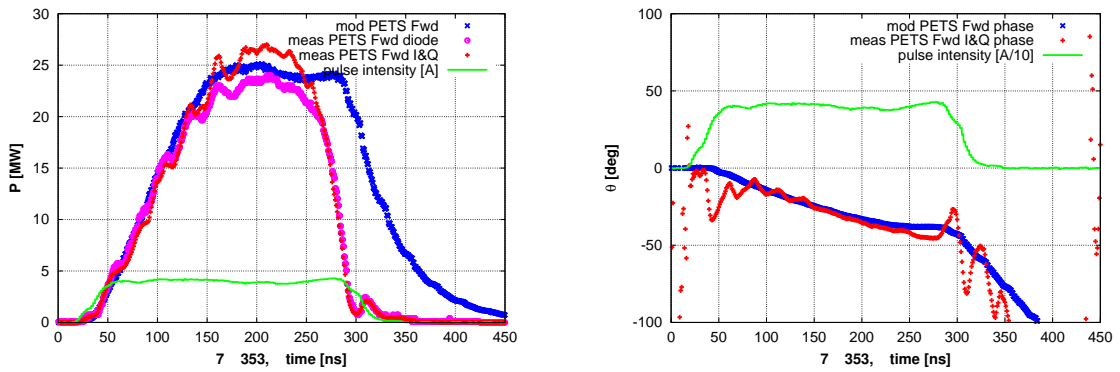


Figure 28: Pulse with pulse-shortening, with field phase starting to oscillate around time of pulse-shortening. From the 16:02 series. Reconstructed and measured RF power (left) and phase (right). Reconstruction using the model in blue (x). Diode power signal in magneta (o). I&Q channel signals in red (+). BPM intensity in green (-).

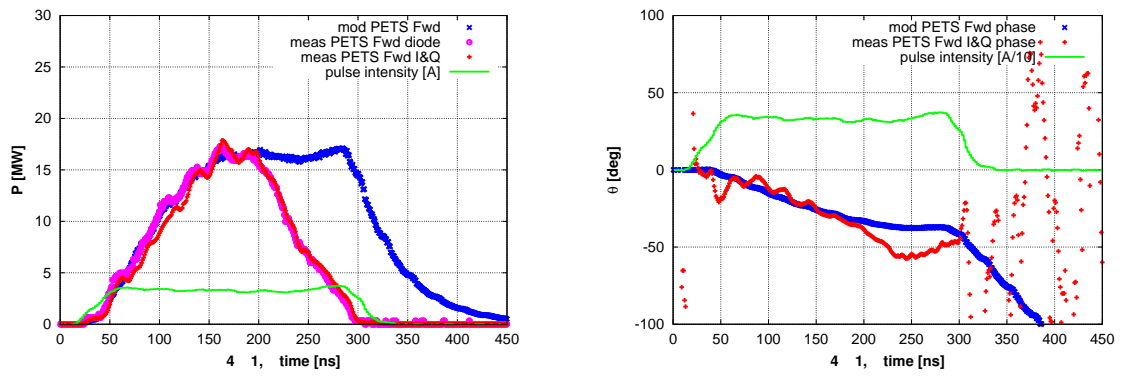


Figure 29: Pulse with pulse-shortening, with field phase increasing around time of pulse-shortening. First pulse from the 14:20 series. Reconstructed and measured RF power (left) and phase (right). Reconstruction using the model in blue (x). Diode power signal in magneta (o). I&Q channel signals in red (+). BPM intensity in green (-).

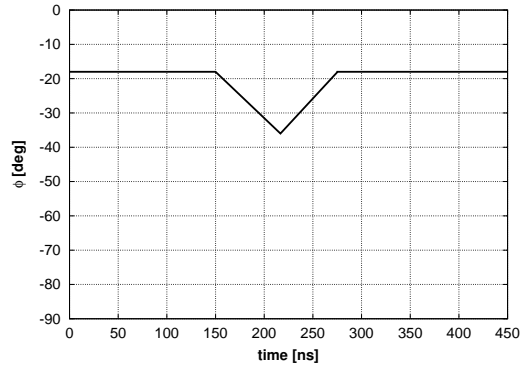


Figure 30: Phase-dip introduced in the recirculation phase in order to fit the measured field phase for a selected pulse with pulse-shortening

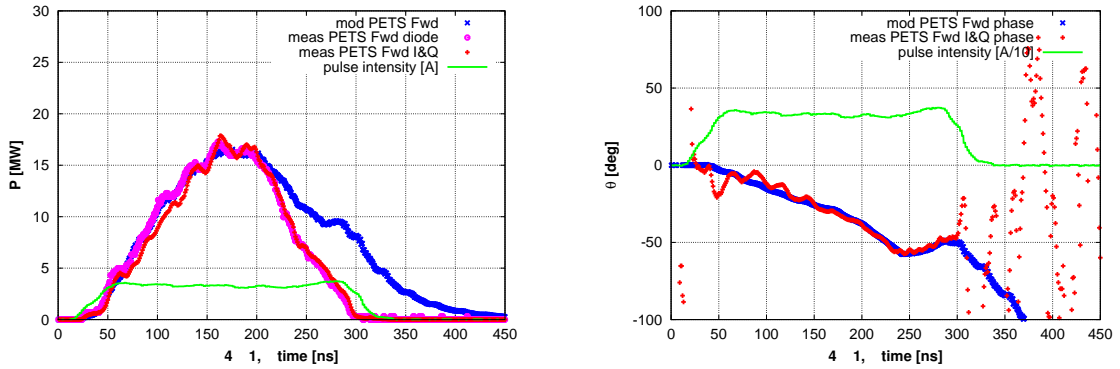


Figure 31: Pulse with pulse-shortening, where the reconstructed field phase is fitted to the measured by introducing a phase-dip in the recirculation phase. First pulse from the 14:20 series. The same pulse, reconstructed with a constant recirculation phase, is presented in Figure 29. Reconstructed and measured RF power (left) and phase (right). Reconstruction using the model in blue (x). Diode power signal in magenta (o). I&Q channel signals in red (+). BPM intensity in green (-).

8 Conclusions

Our minimal model approach has shown, after doing an extensive fit to identify the unknown parameters c , g and ϕ , to give a reasonable correspondence between the reconstructed RF and the measured RF in a part of the day when the CTF3 machine was run under relatively stable conditions. Simple analytical expressions have been developed to calculate the steady state power and field for arbitrary recirculator parameters.

A comparison between the amplitudes of the reconstructed and measured power is impeded by the lack of a precise bunch-length measurement. However, the discrepancy seems to be no more than 30% even if we assume a CTF3 scenario with a short bunch and perfect bunch phasing (the most conservative case for this comparison).

The diode measurements indicate a peak RF power production during the logged part of the run of about 30 MW.

At the first part of the same day of the run the minimal model did not give a satisfying correspondence, neither after applying a new parameter fit. There are clear indications that this might be due to non-ideal bunch phasing, but this should be investigated further.

A large number of pulses with pulse-shortening were logged. The field phase shows a very different behaviour for these pulses (decline, rise or oscillation with respect to the reconstructed phase). An attempt was made to reconstruct the RF power by varying the recirculation phase alone, but the result was negative.

As for the instrumentation, it might seem like the BPM effective bandwidth is lower than the reported. The I&Q demodulator measurements indicate a significant non-linearity with amplitude, more than the diode, and a more appropriate attenuation as well as precise calibration over the full range is recommended for the next TBTS run. Apart from the scaling, the I/Q derived power showed reasonable consistency with the diode measurement.

Finally, since the model used for RF reconstruction is based on the same "sausage model" approach as in PLACET, this work has allowed a first benchmarking of the CLIC decelerator simulation studies.

8.1 Recommendations for future work

We believe that if more sophisticated reconstruction techniques are performed, one might improve the correspondence between power reconstruction and measurement with respect to the results reported in this note. For instance, one might hope to reconstruct the characteristic oscillations of the field phase at the start of the phase measurements. Further work would typically involve one or more of the following items, each requiring a separate effort, and for the moment to be studied further :

- Use of realistic wake functions based on RF simulations (in this note the sausage-model approach was used). This would typically require calculations of wake functions for the full system, plus an upgrade of the tracking code PLACET in order to accommodate the use of arbitrary wake functions.
- Take into account realistic bunch phasing in the CLEX beam (in this note we assumed perfectly synchronous bunches). This would typically require further study of the integrated CTF3 beam dynamics.
- Take into account realistic bunch form-factors, as well as eventual changes in the form-factor along the pulses (in this note we assumed all bunches equal, and we fitted one global constant, including the form-factor). This would typically require further study of the integrated CTF3 beam dynamics as well as more precise bunch measurements.
- In general, the tracking code PLACET could be integrated into the reconstruction process, and integrated studies taking all the above three items into account could then be performed (in this note we have not used PLACET for the reconstruction, only the simple formulae developed within this note). This would typically require constructing PLACET models for all of the CTF3, with appropriate upgrades of PLACET where needed.

Considering the importance of understanding fully the details of the beam generated power production, which is a key concept of CLIC, we would consider the items proposed here to be worthwhile the effort.

9 Acknowledgements

Acknowledgements goes to Roger Ruber for swift answers to all questions about the TBTS and the instrumentation and for providing the front page latex template; to Roger Ruber and Volker Ziemann for useful discussions along this work. Furthermore Daniel Schulte for physics discussions, Alexey Dubrovskiy for software discussions and Simona Bettoni for steady operation. Finally Steffen Doebert for RF calibration and explanations, Anne Dabrowski for CTF3 beam measurements and of course Igor Syrathev - the PETS master.

References

- [1] I. Syratchev et al., High RF Power Production for CLIC, *CERN CLIC Note 720* and *Proceedings of PAC'07*, WEPMN071 (2007)
- [2] R.J.M.Y. Ruber et al., The CTF3 Two-Beam Test-Stand Installation and Experimental Program, *Proceeding of EPAC'08*, WEPP139 (2008)
- [3] G. Geschonke, A. Ghigo (ed.) et al., "CTF3 Design Report", CERN/PS 2002-008(RF), LNF-02/008(IR).
- [4] I. Syratchev et al., CLIC RF High Power Production Testing Program, *Proceeding of EPAC'08*, WEOBG01 (2008)
- [5] D. Schulte, The Tracking Code PLACET, <https://savannah.cern.ch/projects/placet/>
- [6] A. Millich and L. Thorndahl, Loss factor Dependence on Group Velocity in Disk-Loaded Travelling-Wave Structures, *CERN CLIC Note 366* (1999)
- [7] I. Syratchev, PETS and drive beam development for CLIC, X-Band RF Structure and Beam Dynamics Workshop (2008), <http://indico.cern.ch/event/39372>
- [8] Anne Dabrowski, private communication
- [9] M. Gasior, An Inductive Pick-Up for Beam Position and Current Measurements, *Proceeding of DIPAC'03*, CT01 (2003)
- [10] R. Ruber, Two-beam Test-stand Instrumentation Layout, CERN EDMS document 894313 version 4, <https://edms.cern.ch/document/894313/4>
- [11] Roger Ruber, private communication
- [12] Igor Syratchev, private communication
- [13] Acqiris DC270, <http://cern.ch/ctf3-tbts/instr/DC265-270.pdf>
- [14] W.H. Press et al., Numerical Recipes, 3rd Edition, Cambridge University Press (2007)
- [15] V. Ziemann, Data Analysis for PETS Recirculation, CERN CTF3-Note-094 (2009)
- [16] http://elogbook/eLogbook/event_viewer.jsp?eventId=1162471

A Estimation of the PETS output field and power

In this section we will derive (well known) formulae for the PETS steady state output field, voltage and power from basic principles, based on a "sausage model". By sausage model we mean that wake fields trail particles like sharply cut sausages, and that these fields are coupled out from or in to structures with an infinite bandwidth.

The PETS is characterised by the high group-velocity and the fact that the beam generates the field. This implies that the formulae developed here will differ somewhat from that of standard structures. All of this section is concerned with the PETS operating without field recirculation.

The "sausage model" approach has already been introduced in [5]. The introduction of the field compression factor below has been discussed in [6], but no documents have been found that clearly present the full discussion of field, power and decelerating integrated field, thus the raison d'être for this section. We will assume an ideal, uniform bunch-train, and in-phase power production. We take the usual assumption of an ultra-relativistic beam with a particle β equal to 1.

A.1 Basic concepts

When a charge passes through the PETS an RF field will be generated by the impedance and travel along the PETS with a group velocity $v_g < c$. When the particle has reached the PETS output at distance L , the field will have travelled a distance $\frac{v_g}{c}L \equiv \beta_g L$. This is illustrated by Figure 32 (for illustrational purposes the figure parameters in this section use a PETS length $L = 1$, a group velocity of $v_g \approx 0.75c$ and a bunch frequency of $f_{bunch} \approx 1.5$ GHz).

A.2 Quantities defining a structure

For a periodic structure we can define the following quantities :

- 1) The shunt-impedance per unit length

$$R' = \frac{(\text{effective longitudinal electric field})^2}{\text{power loss per unit length}} = \frac{E^2}{\mathcal{P}'} \quad (8)$$

- 2) The quality factor

$$Q = \frac{\text{stored field energy per unit length}}{\text{ohmic loss per unit length per radian of RF oscillations}} = \frac{\mathcal{E}'}{\mathcal{P}' \omega_{RF}} \quad (9)$$

where \mathcal{P}' and \mathcal{E}' denote respectively power loss per unit length and stored energy per unit length. In general we will denote quantities per unit length by a prime ($'$).

For a structure with a sharply peaked (high Q) fundamental mode, the impedance of this mode will be proportional to the ratio (R'/Q) , in this note given in [linac- Ω /m].

The corresponding longitudinal loss factor per unit length is defined as the energy a point-charge loses to the impedance, per unit length, normalised to the charge squared. It can be calculated from an RLC-circuit description of the mode, yielding $k'_{|v_g \rightarrow 0} \equiv \frac{\mathcal{E}'}{q^2} = \frac{1}{4}(R'/Q)\omega_{RF}$ [V/C/m]. The energy lost to the impedance is converted into a wake field trailing the charge; in the case of the PETS, a 12 GHz RF field.

For structures with high group velocity the energy in the field will be concentrated in a fraction $(1 - \beta_g)$ of the structure length, as illustrated in Figure 32, implying that the loss factor per unit length must be scaled by $\frac{1}{1 - \beta_g}$ in order to obey energy conservation [6]. The PETS loss factor should per unit length thus be expressed as

$$k' = \frac{1}{4}(R'/Q)\omega_{RF} \frac{1}{1 - \beta_g}$$

The average force of the wake field per unit length on a witness particle with charge q_w trailing a source point charge q_s , normalised to both charges, is defined as the longitudinal wake function per unit length $w'_0(z)$ [V/C/m]. The wake function depends on the distance z between the two particles, and for a sharply peaked mode it is given by

$$W'_0(z) = 2k' \cos\left(\frac{\omega_{RF}}{c}z\right) = \frac{1}{2}(R'/Q)\omega_{RF} \cos\left(\frac{\omega_{RF}}{c}z\right) \frac{1}{1 - \beta_g} \quad (10)$$

The factor 2 enters because the driving charge sees only half of the field it generates, while a trailing charge will see the full field.

Computer codes are used to calculate $W'_0(z)$ (time-domain codes) or the corresponding structure impedance (frequency-domain code). The two quantities are Fourier transform pairs and contain therefore the same information.

A.3 PETS field amplitude

We start by estimating the longitudinal electric field amplitude (denoted simply "the field" in this note) originating from a point-like bunch (plb) q_b . For the PETS we consider only the sharply peaked 12 GHz fundamental mode, and the field is therefore equivalent to the wake function per unit length, multiplied by the driving charge

$$E_{plb} = q_b W'_0(0) = \frac{1}{2}q_b(R'/Q)\omega_{RF} \frac{1}{1 - \beta_g}$$

For a long structure ohmic losses become significant. For a given structure length their effect can be taken into account by incorporating an ohmic loss reduction factor, $\eta_{\Omega, PETS}$, in the field expressions³

³the factor can be calculated from the mode Q, for the PETS estimated to $Q \approx 7200$

$$E_{plb} \rightarrow E_{plb} \eta_{\Omega, PETS}$$

If the bunch has a finite length, the field originating from this bunch is found by summing over the charge distribution $\lambda(z)$

$$E_{bunch} = q_b \int_{-\infty}^{\infty} dz' \lambda(z') W'_0(z' - 0) \equiv E_{plb} F(\lambda)$$

which defines the symmetric charge-distribution form factor

$$F(\lambda) \equiv \int_{-\infty}^{\infty} dz' \lambda(z') \cos\left(\frac{\omega_{RF}}{c} z'\right) \quad (11)$$

For an e.g. Gaussian bunch the form factor evaluates to $F(\lambda(\sigma_z)) = \exp(-\frac{1}{2}(\sigma_z \omega_{RF}/c)^2)$.

The RF field will reach steady-state when a trailing bunch catches up with the end of the field of the first bunch at the PETS output, as illustrated in Figure 33 (fields of bunches trailing the bunch at the PETS end are not shown, because they do not contribute to the PETS output field). The fill-time, defined here as the time between first RF at PETS output until steady-state, is therefore given by

$$t_{fill} \equiv \frac{L}{v_g} (1 - \beta_g)$$

and the number of trailing bunches before this condition is reached

$$N_{fill} \equiv t_{fill} f_{bunch} = \frac{L f_{bunch}}{v_g} (1 - \beta_g)$$

At steady state the field originating from N_{fill} bunches will be superpositioned at the field output, yielding the steady state beam generated field

$$E_{beam} = N_{fill} E_{bunch} = \frac{1}{2} (R'/Q) \omega_{RF} \frac{L}{v_g} IF(\lambda) \eta_{\Omega, PETS} \quad (12)$$

A.4 PETS output power

From Eqs. (8) and (9) we can express R'/Q as

$$(R'/Q) \omega_{RF} = \frac{E^2}{\mathcal{E}'}$$

showing how the average longitudinal field and the average stored field energy per unit length are linked through (R'/Q) .

The PETS output field calculated in Eq. (12) is coupled out and exits the PETS with the group velocity v_g . The PETS output power can be found by evaluating the power flow out of the PETS

$$\begin{aligned}
P &\equiv \frac{d\mathcal{E}}{dt} = \frac{d\mathcal{E}}{ds} \frac{ds}{dt} = \mathcal{E}' v_g = \frac{E_{beam}^2}{(R'/Q)\omega_{RF}} v_g \\
&= \frac{1}{4} (R'/Q) \frac{\omega_{RF}}{v_g} L^2 I^2 F^2(\lambda) \eta_{\Omega, PETS}^2
\end{aligned} \tag{13}$$

A.5 PETS integrated field

The longitudinal field as seen by a witness particle builds up step-wise as the fields from leading bunches are caught up with (Figure 33) and the peak integrated field can therefore be estimated as

$$\hat{U} = \frac{1}{2} E_{beam} L$$

or, if one wants to estimate \hat{U} from P , 13 yields the following relation

$$\hat{U}^2 = \frac{1}{4} L^2 \frac{(R'/Q)\omega_{RF}}{v_g} P \tag{14}$$

The integrated field as seen by a witness particle is different from the voltage across the PETS at a snapshot in time, again due to the significant group velocity. The value of \hat{U} in [V] corresponds to the peak deceleration of trailing particles in [eV], if single-bunch effects are ignored.

We note that the \hat{U} is related to the mean voltage seen by the particles $\langle U \rangle = \frac{P}{I\eta_{\Omega, PETS}} = \frac{1}{2} E_{beam} L F(\lambda)$ by a factor

$$\hat{U} = \langle U \rangle F(\lambda)$$

A.6 Circuit-ohm convention versus linac-ohm convention

The derivations above assume that R'/Q is given in linac- Ω/m (commonly used when working with Linacs), while circuit- Ω/m is also being used in the accelerator community. The relation is

$$\frac{R'}{Q} |_{\text{Linac-}\Omega/m} = 2 \frac{R'}{Q} |_{\text{Circuit-}\Omega/m}$$

implying that the formulae for E , P and U should be scaled by a factor 2 if R'/Q is given in circuit- Ω/m . For instance, in [6] the formulae are given in Circuit- Ω/m .

In the circuit-ohm convention the R in R/Q is the shunt impedance of the RLC-circuit description of the mode. For alternating fields we would get a factor 1/2 in the definitions of R and R/Q originating from Eq. (8) if they would be given in circuit-ohm. In Linacs we almost

exclusively deal with alternating fields in structures, and therefore it has been found more convenient to include the factor $1/2$ in the definitions of R (and R/Q), leading to the linac-ohm convention.

A.7 Limitations and corrections to the simple expressions

A.7.1 Structure length versus bunch-to-bunch spacing

If the structure is short with respect to the bunch-to-bunch spacing, say a few distances, it is clear that the expressions above break down. E.g. a structure length difference of only one bunch-to-bunch spacing can decide whether another trailing bunch will add to the maximum field or not. Therefore the formulae above are only good approximations for large $N_{fill} \gg 1$.

A.7.2 Single-bunch effects

In Eq. (11) the lower integration limit should for the first-bunch be z when calculating the deceleration and the power. In addition the single-bunch wake will influence the calculation of \hat{U} for very short bunches. However, if $N_{fill} \gg 1$ and if the bunch is sufficiently long, the corrections to the formulae above will be small. If not, an efficiency "fudge-factor" should be included to take this effect into account.

A.8 Numerical estimations using PLACET

The quantities estimated in Eqs. (12), (13) and (14) are based on a simple model, but will give precise answers for long enough structures and bunches (to be quantified below).

If better accuracy is desired the tracking code PLACET [5] includes functions to calculate Eqs. (13) and (14) taking into account an arbitrary charge distribution and including the effect of short structures and single-bunch effects. In PLACET, however, instant field fill and drain-out are still assumed. Eventually one can resort to complete structure simulations codes.

We have verified the applicability of Eqs. (13) and (14) with respect to the PLACET functions. In Figure 34 the comparison is done with a 1 m long structure with $f_{bunch} = 12$ GHz, and by varying the RMS length for Gaussian bunches. We see that for $\sigma_z > 1$ mm both the error in voltage and in power are within 3 %. The power does not depend on the relative contribution of the self-wake, and is therefore almost flat.

In Figure 35 the comparison is done with $\sigma_z = 1$ mm, $f_{bunch} = 12$ GHz, and by varying the structure length. We see that for $L > 0.5$ m the error in voltage is within 1 % and the error in power within 0.5 %. The oscillation of the power ratio with length is due to the fact that the analytic expression is linear while the simulated takes into the account that N_{fill} increase step-wise, smoothed by the bunch-length. How much of these oscillations are due to the sausage model approach and how much will remain if we compare the linear formula to full system simulations is to be studied.

Nevertheless, this discussion shows that the formulae presented in this appendix are, for the TBTS set-up, precise to within 1 % with respect to the PLACET estimates.

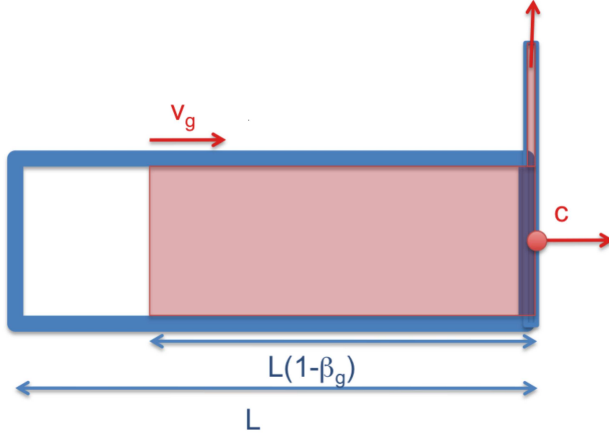


Figure 32: PETS field from one charge

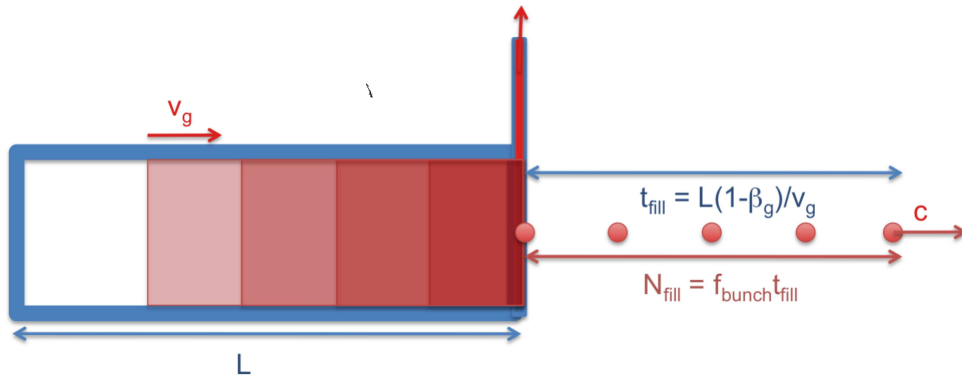


Figure 33: PETS completely filled, after a time t_{fill} , with N_{fill} bunches contributing

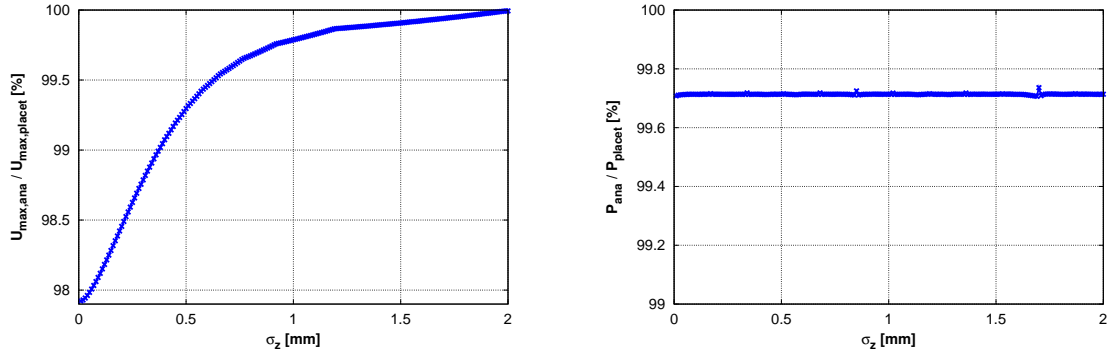


Figure 34: Ratio of calculated versus simulated maximum voltage (left) and produced power (right), for a 1 m structure and varying bunch RMS length

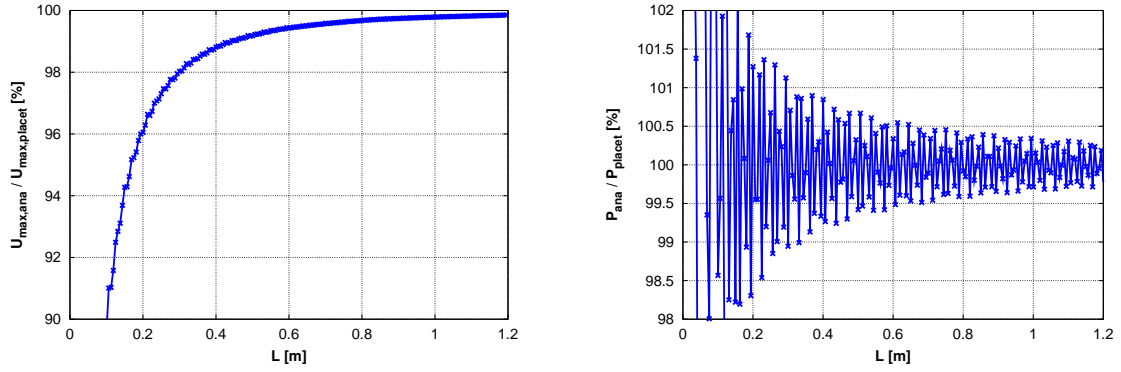
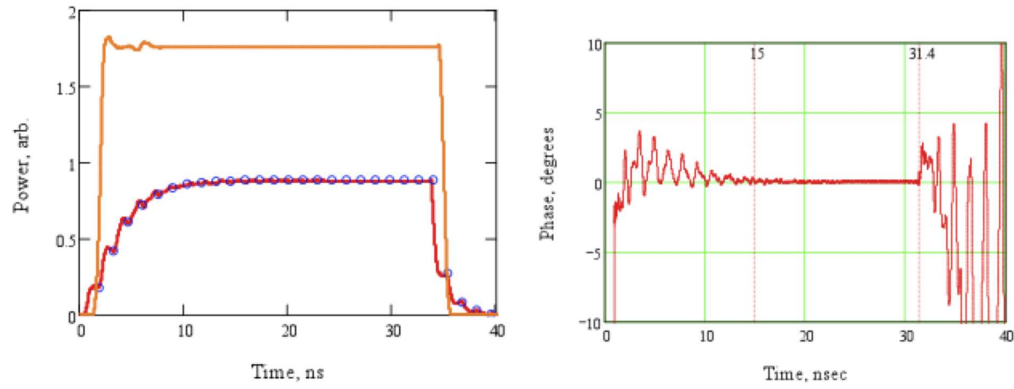


Figure 35: Ratio of calculated versus simulated maximum voltage (left) and produced power (right), for a 1 mm RMS bunch length and varying structure length

B Example reconstruction using full GdfidL PETS model

The following graphs (Courtesy of I. Syratchev) show an example of power and phase for a PETS with recirculation, where a realistic RF model of the whole system has been simulated using GdfidL. Note that neither the system simulated nor the recirculator parameters are the same as discussed in this note.



C Mapping between graph series number and data log folder names

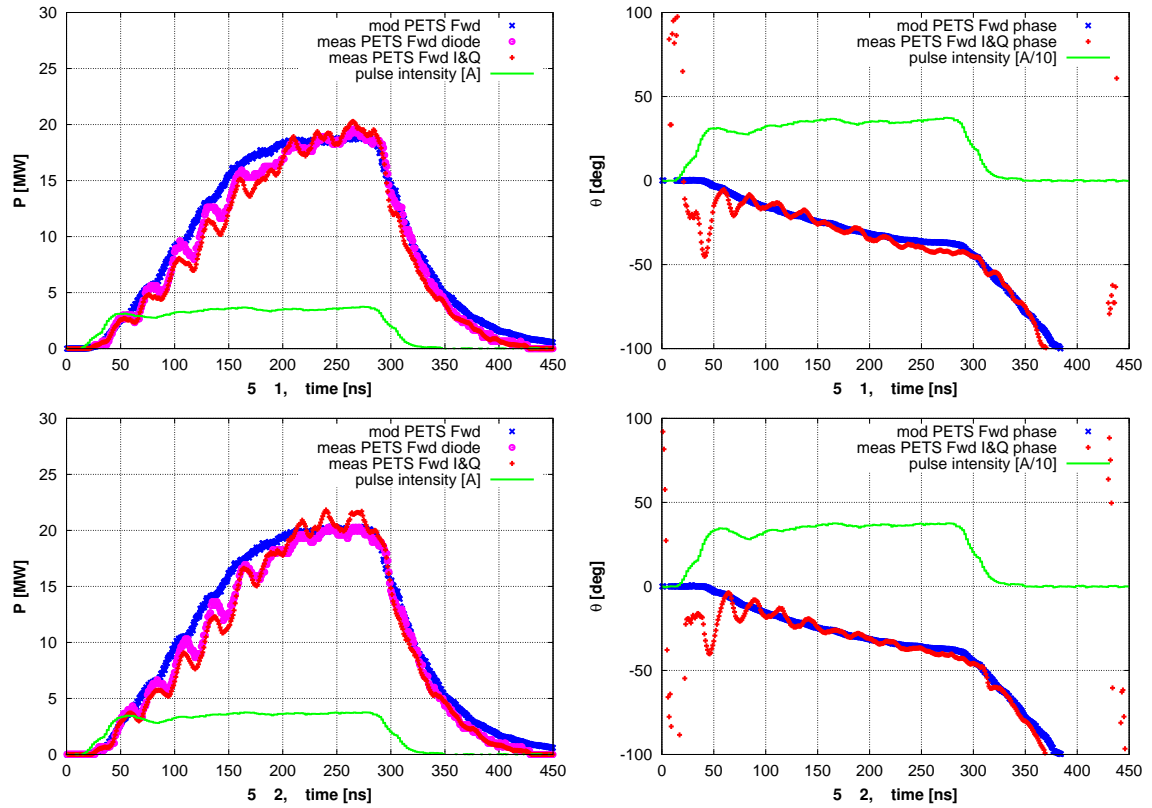
For identification purposes each measured pulse in this note is marked, at the start of the x-axis, with a series number and a pulse number within that series. Below details about each series are listed.

series nr	folder name	start of logging	notes taken
9	GOOD5A_2/	17:13	poor fit, too low power - check CALIB BUT, possible reason after control system failure avg. wrong
8	GOOD5A/	17:05	poor fit, too low power - check CALIB BUT, possible reason after control system failure avg. wrong
7	BREAKS/	16:02	up to 350 perfect, by fit)
6	BREAK19/	15:48	perfect - but look at single break at pulse 91 (scan e.g. 88-92)
5	GOODML4/	15:36	perfect
4	GOODML3/	14:20	good fit at start, but pulse shortening
3	GOOD_WP/	13:23	good fit at start, but pulse shortening / clearly different phase!
2	GOODML2/	12:32	poor fit also at start, but pulse shortening) - VERIFY CALIB!!
1	GOODML1/	12:16	poor fit also at start, but pulse shortening) - VERIFY CALIB!!

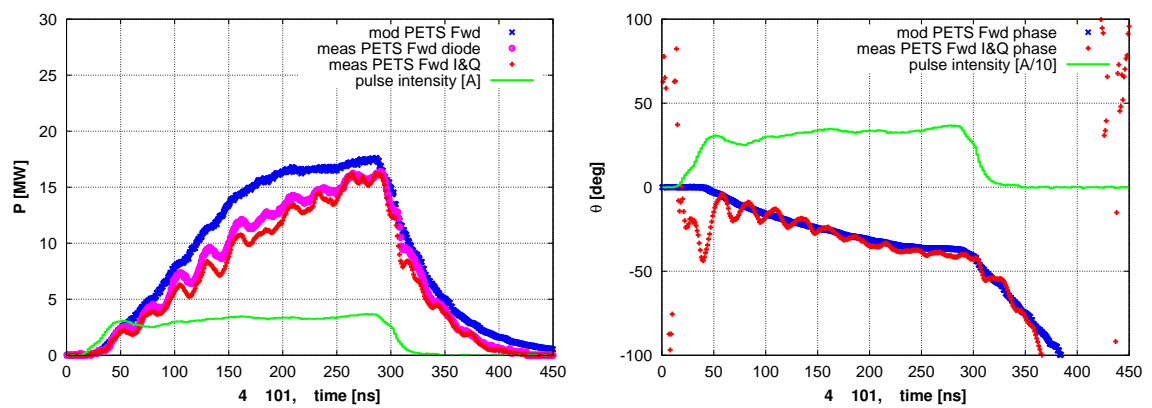
D Reconstruction of additional pulses

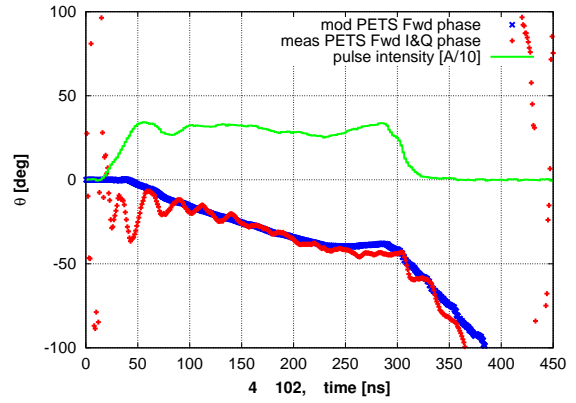
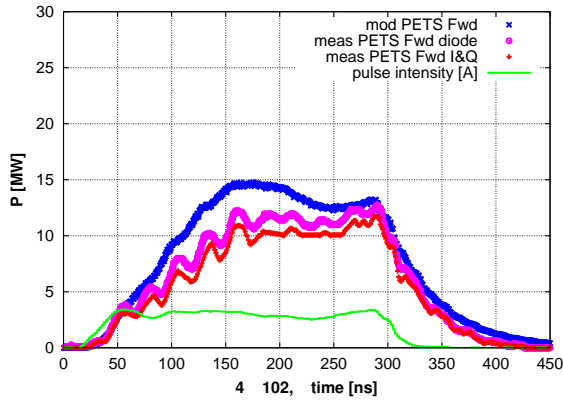
D.1 More pulses logged after klystron phase optimisation

Start of 15:36 series :



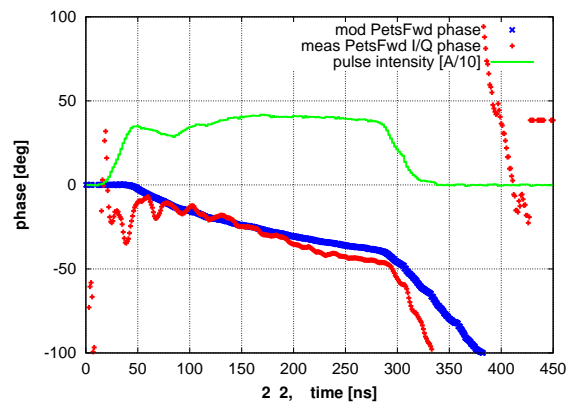
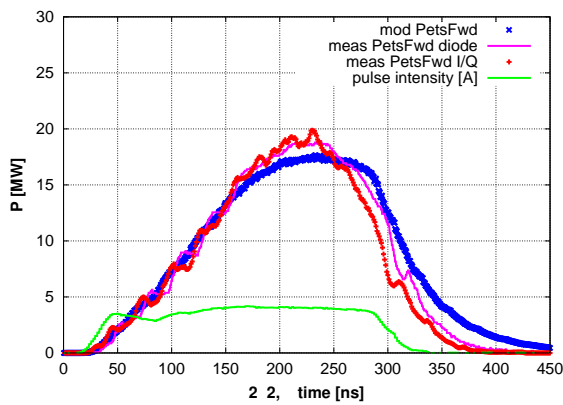
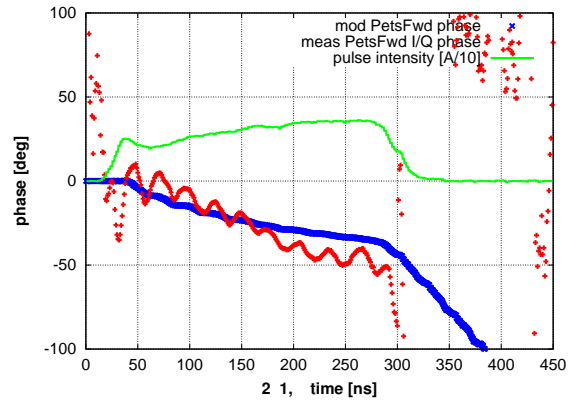
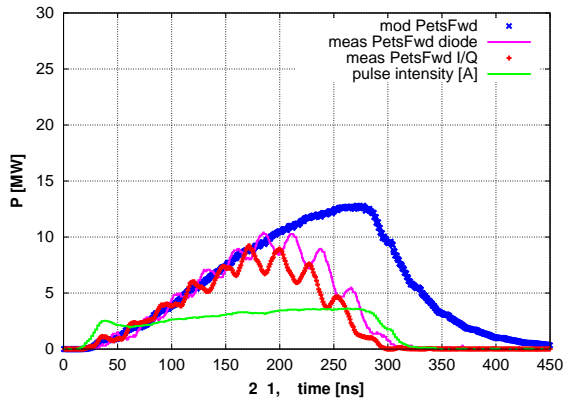
Into the 14:20 series (*Start* of series is flawed with pulse-shortening; see below):



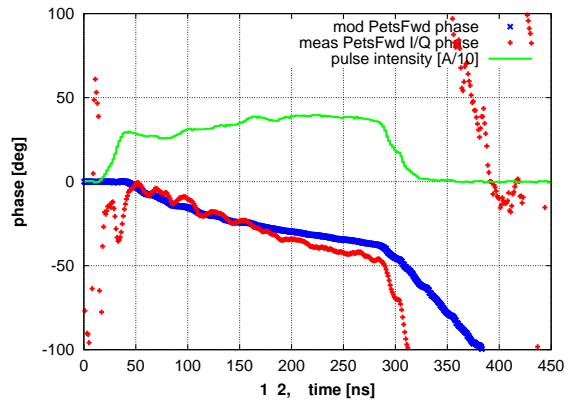
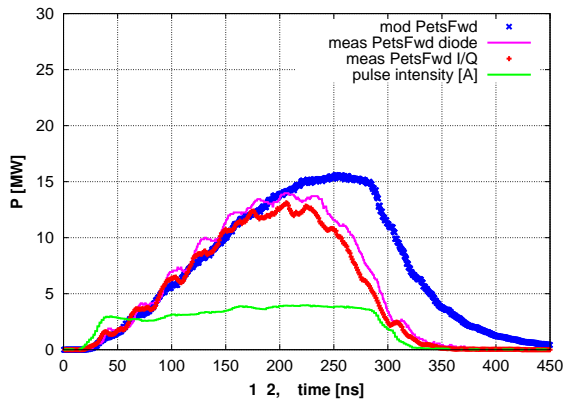
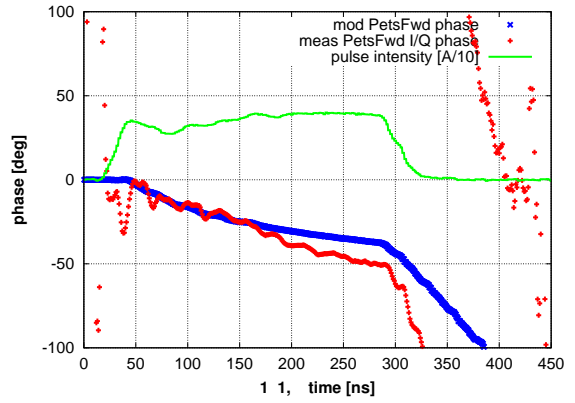
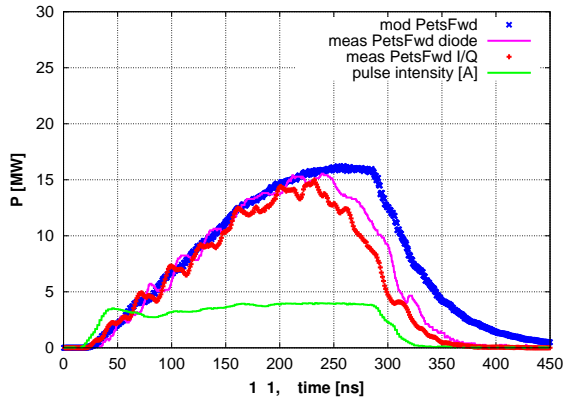


D.2 More pulses logged before klystron phase optimisation

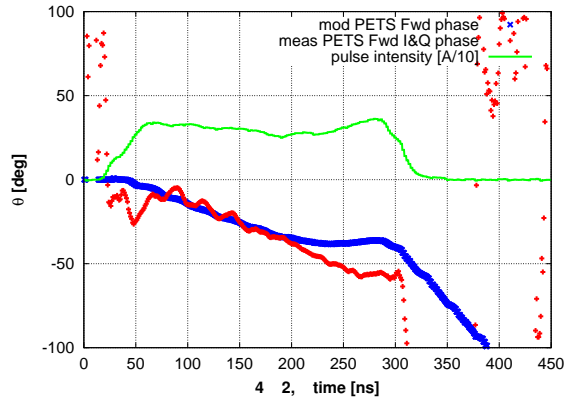
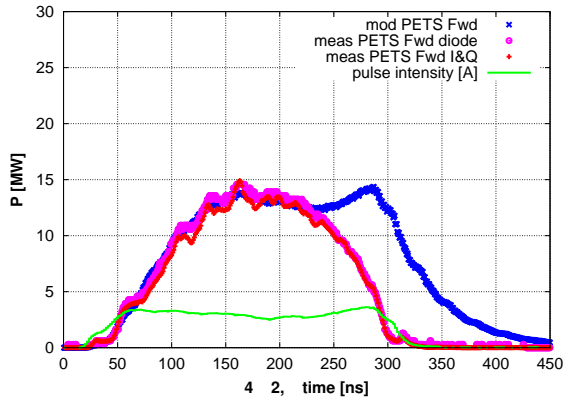
Start of 12:32 series (different hardware attenuation has been compensated for) :

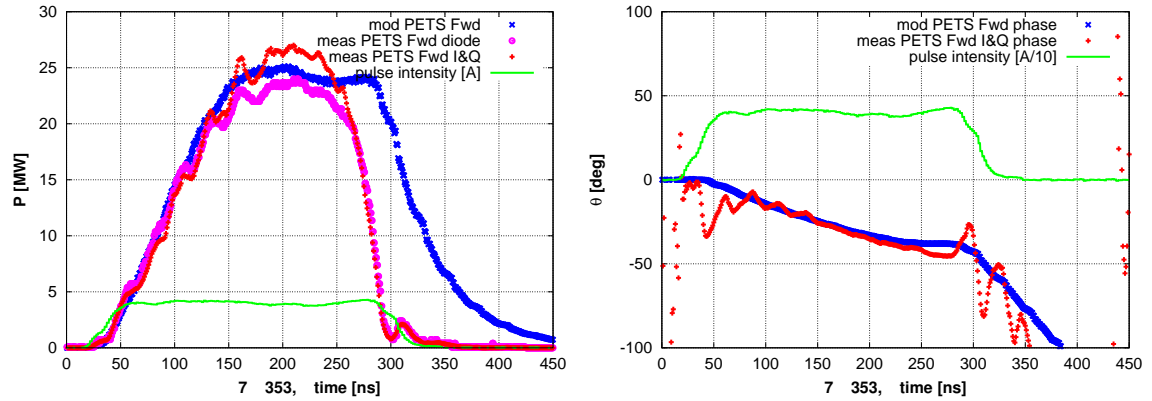


Start of 12:16 series (different hardware attenuation has been compensated for) :



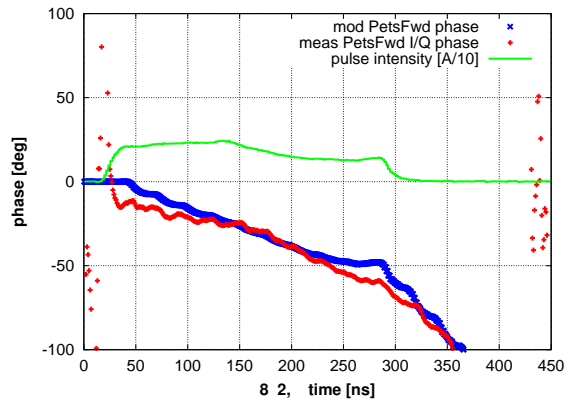
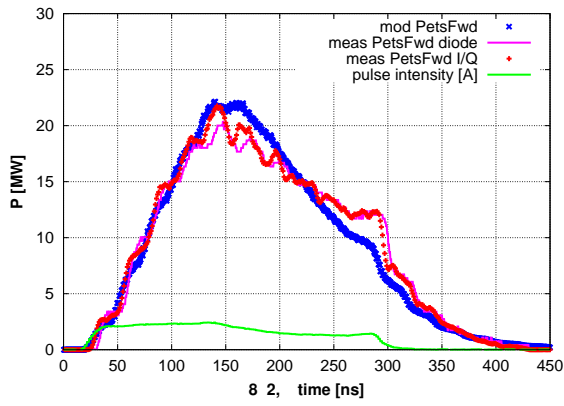
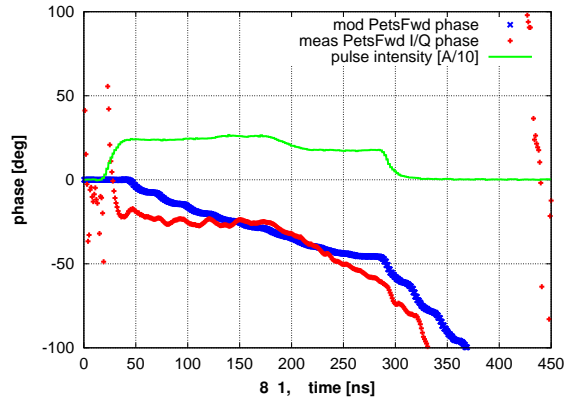
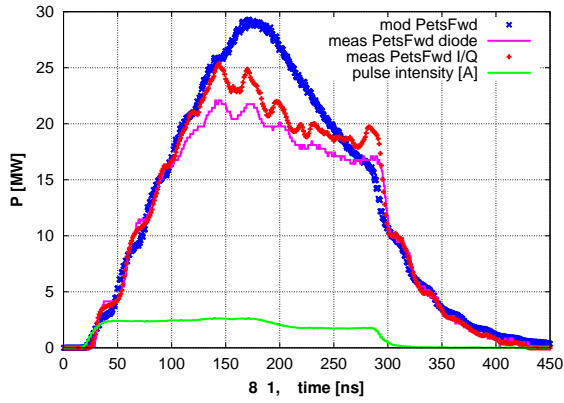
D.3 More pulses with pulse-shortening





D.4 Pulses with three times combination after machine reset

Towards the end of the day a beam with three times recombination in the combiner ring was set up. Unfortunately, just afterwards there was a serious control system failure resulting in reset of many of the machine control system values. After this event, all the logged TBTS BPM data were significantly smaller than what was read in the control room. This was discovered only later when analysing the data, and it is not fully understood why. For completeness we do include some pulses from this data series as well here, but due to the uncertainties with these data no attempt is done to interpret the results here. The intensity in green is what was logged, but we have scaled the corresponding field by a factor 1.7.



E Key plots without I&Q power

Here we include some of the key plots shown earlier, but with-out the apparently non-linear I&Q power graph included, for the purpose of future re-use. Also included is the reconstructed power for a scenario without recirculation.

